

1 **Bayesian calibration of the Mg/Ca paleothermometer**
2 **in planktic foraminifera**

3 **Jessica E. Tierney¹, Steven B. Malevich¹, William Gray², Lael Vetter¹ &**
4 **Kaustubh Thirumalai¹**

5 ¹University of Arizona Department of Geosciences, 1040 E 4th St Tucson AZ 85721

6 ²Laboratoire des Sciences du Climat et de l'Environnement (LSCE/IPSL), Gif-sur-Yvette, France

7 **Key Points:**

- 8 • We introduce Mg/Ca Bayesian calibrations for planktic foraminifera
9 • Hierarchical modeling is used to constrain multivariate Mg/Ca sensitivities
10 • For deep-time applications, we incorporate estimates of Mg/Ca of seawater

Corresponding author: Jessica Tierney, jesst@email.arizona.edu

Abstract

The Mg/Ca ratio of planktic foraminifera is a widely-used proxy for sea-surface temperature, but is also sensitive to other environmental factors. Previous work has relied on correcting Mg/Ca for non-thermal influences. Here, we develop a set of Bayesian models for Mg/Ca in planktic foraminifera that account for the multivariate influences on this proxy in an integrated framework. We use a hierarchical model design that leverages information from both laboratory culture studies and globally-distributed core top data, allowing us to include environmental sensitivities that are poorly constrained by core top observations alone. For applications over longer geological timescales, we develop a version of the model that incorporates changes in the Mg/Ca ratio of seawater. We test our models – collectively referred to as BAYMAG – on sediment trap data and on representative paleoclimate time series and demonstrate good agreement with observations and independent SST proxies. BAYMAG provides probabilistic estimates of past temperatures that can accommodate uncertainties in other environmental influences, enhancing our ability to interpret signals encoded in Mg/Ca.

Plain Language Summary

The amount of magnesium (Mg) incorporated into the calcite shells of tiny protists called foraminifera is determined by the temperature of the water in which they grew. This allows paleoclimatologists to measure the magnesium-to-calcium (Mg/Ca) ratio of fossil foraminiferal shells and determine how past sea-surface temperatures (SSTs) have changed. However, other factors can influence Mg/Ca, like the salinity and pH of seawater. Here, we develop Bayesian models of foraminiferal Mg/Ca that account for all of the influences on Mg/Ca and show how we can use these to improve our interpretations of Mg/Ca data.

1 Introduction

The magnesium-to-calcium (Mg/Ca) ratio of planktic foraminifera is a commonly-used proxy method for reconstructing past sea-surface temperatures (SSTs). It has played a pivotal role informing our understanding of tropical climate dynamics in the Late Quaternary (Lea et al., 2000, 2003; Rosenthal et al., 2003; Stott et al., 2007) as well as in deeper geologic time (e.g., Evans et al., 2018). The proxy has theoretical basis in thermodynamics, which predicts a non-linear increase in Mg incorporation into calcite as temperatures rise (Oomori et al., 1987). Laboratory culturing of planktic foraminifera confirms an exponential dependence of Mg/Ca on temperature, albeit with a stronger sensitivity than thermodynamic predictions, indicating that biological “vital effects” also play a role (Nürnberg et al., 1996; Lea et al., 1999). Laboratory experiments also demonstrate that Mg/Ca in foraminifera is sensitive to other environmental factors, such as salinity and pH (Lea et al., 1999; Kiskakürek et al., 2008; Dueñas-Bohórquez et al., 2009; Hönisch et al., 2013; Evans, Wade, et al., 2016). The extent to which these secondary factors influence or compromise SST prediction from Mg/Ca is an ongoing topic of investigation (Ferguson et al., 2008; Mathien-Blard & Bassinot, 2009; J. Arbuszewski et al., 2010; Hönisch et al., 2013; Evans, Wade, et al., 2016; Gray et al., 2018; Gray & Evans, 2019). Beyond competing environmental factors, the depositional environment also influences Mg/Ca. If the calcite saturation state of the bottom waters is low, partial dissolution of foraminiferal calcite occurs, lowering Mg/Ca (Brown & Elderfield, 1996; Rosenthal et al., 2000; Regenberg et al., 2006, 2014).

Previous calibrations for Mg/Ca have been based on either laboratory culturing experiments (Nürnberg et al., 1996; Lea et al., 1999; Gray & Evans, 2019), sediment trap data (Anand et al., 2003; Gray et al., 2018) or modern core tops (Elderfield & Ganssen, 2000; Dekens et al., 2002; Khider et al., 2015; Saenger & Evans, 2019). Culture experiments provide precise constraints on environmental sensitivities, but are limited in that

laboratory conditions are not perfect analogs for the natural environment. Sediment traps have an advantage in that seasonality of foraminiferal occurrence and corresponding ocean temperatures are well-constrained, but they do not account for the effects of dissolution or bioturbation. Sedimentary core tops integrate effects associated with both occurrence and preservation, and are thus better analogs for the conditions typical of the geological record, but uncertainties in seasonal preferences and the depth of calcification can in some cases lead to misleading inference of secondary environmental sensitivities (Hönisch et al., 2013; Hertzberg & Schmidt, 2013).

Here, we use both core top and laboratory culture data to develop a suite of Bayesian hierarchical models for Mg/Ca. We collate over 1,000 sedimentary Mg/Ca measurements to formulate new calibrations for four major planktic groups: *Globigerinoides ruber* (including both pink and white chromotypes), *Trilobatus sacculifer*, *Globigerina bulloides*, and *Neogloboquadrina pachyderma* (including *N. incompta*). First, we assess the impact of adding known secondary environmental predictors (bottom water saturation state, salinity, pH and laboratory cleaning technique) to a Mg/Ca calibration model. We then compute both pooled (all species groups considered together) and hierarchical (species groups considered separately) calibration models using Bayesian methodology similar to that previously developed for core top models of planktic foraminiferal $\delta^{18}\text{O}$ (Malevich et al., 2019). We assess the validity of the new regressions by applying them to sediment trap data and downcore measurements of foraminiferal Mg/Ca. Given that planktic foraminiferal Mg/Ca is increasingly used for SST estimation in deeper geological time, we develop a version of our model that accounts for secular changes in the Mg/Ca composition of seawater. The overarching goal of this study is to develop a flexible set of forward and inverse models for planktic foraminiferal Mg/Ca that estimate observational uncertainties and can be used in a variety of paleoclimatic applications, including inter-proxy comparisons, proxy-model comparisons, and data assimilation.

2 Data compilation

We compiled 1250 core-top Mg/Ca measurements from the literature (Rosenthal & Boyle, 1993; Russell et al., 1994; Brown & Elderfield, 1996; Hastings et al., 1998; Mashiotta et al., 1999; Elderfield & Ganssen, 2000; Ganssen & Kroon, 2000; Dekens et al., 2002; Lea et al., 2003; Palmer & Pearson, 2003; Pahnke et al., 2003; Rosenthal et al., 2003; Visser et al., 2003; Schmidt et al., 2004; Barker et al., 2005; Farmer et al., 2005; Keigwin et al., 2005; Oppo & Sun, 2005; Steinke et al., 2005; Sun et al., 2005; Weldeab et al., 2005; Benway et al., 2006; Dahl & Oppo, 2006; Lea et al., 2006; Meland et al., 2006; Regenberg et al., 2006; Weldeab et al., 2006; de Garidel-Thoron et al., 2007; Leduc et al., 2007; Levi et al., 2007; Richey et al., 2007; Stott et al., 2007; Wei et al., 2007; Weldeab et al., 2007; Cléroux et al., 2008; Ferguson et al., 2008; Nürnberg et al., 2008; Steinke et al., 2008; Yu et al., 2008; Kozdon et al., 2009; Mathien-Blard & Bassinot, 2009; Regenberg et al., 2009; Richey et al., 2009; Oppo et al., 2009; J. Arbuszewski et al., 2010; Kubota et al., 2010; Linsley et al., 2010; Marchitto et al., 2010; Mohtadi et al., 2010; Xu et al., 2010; Johnstone et al., 2011; Mohtadi et al., 2011; Sabbatini et al., 2011; Thornalley et al., 2011; van Raden et al., 2011; Boussetta et al., 2012; Fallet et al., 2012; Schmidt, Weinlein, et al., 2012; Schmidt, Chang, et al., 2012; J. A. Arbuszewski et al., 2013; Riethdorf et al., 2013; Saraswat et al., 2013; Aagaard-Sørensen et al., 2014; Dyez et al., 2014; Gibbons et al., 2014; Moffa-Sánchez et al., 2014; Romahn et al., 2014; Weldeab et al., 2014; Khider et al., 2015; Rustic et al., 2015; Gebregiorgis et al., 2016; Parker et al., 2016; Tierney et al., 2016; Vázquez Riveiros et al., 2016; Hollstein et al., 2017; Kristjánsdóttir et al., 2017; Morley et al., 2017). The data collection includes the core name, the site location (latitude, longitude, water depth), the interval of the core sampled (if provided), the Mg/Ca ratio, corresponding $\delta^{18}\text{O}$ and $\delta^{13}\text{C}$ measurements (if provided), the species, the size fraction sampled (if provided) and the source reference. Since previous work points to a systematic offset in Mg/Ca based on the cleaning method used in the laboratory (Rosenthal

113 et al., 2004; Khider et al., 2015), we flagged the data according to the type of cleaning
 114 performed, with a value of 0 assigned to samples cleaned with an oxidative protocol (e.g.,
 115 Barker et al., 2003) and a value of 1 assigned to samples cleaned with an additional re-
 116 ductive step (e.g., Boyle & Keigwin, 1985). We assigned a quality control flag to each
 117 core top – indicating whether the data should be included in our calibration model or
 118 not – based on the interpretation of the data in the original study. For example, data
 119 that were noted as suspect due to small sample size or encrustation of high-Mg coatings
 120 were excluded. We also excluded data from the eastern Mediterranean, where authigenic
 121 high-Mg coatings are commonly observed and result in anomalous Mg/Ca values (Sabbatini
 122 et al., 2011). This initial quality screen reduced our dataset to 1153 samples, with 478
 123 core tops for *G. ruber* white, 74 for *G. ruber* pink, 237 for *T. sacculifer*, 72 for *N. pachy-*
 124 *derma*, 158 for *N. incompta*, and 134 for *G. bulloides* (Fig. 1). *G. ruber* white and pink
 125 core top samples were subsequently combined and averaged and collectively treated as
 126 the *G. ruber* group, recognizing that these chromotypes are closely related genetically
 127 (Aurahs et al., 2011) and have similar geochemistry (Richey et al., 2019, 2012). In ad-
 128 dition, initial exploration indicated that the *G. ruber* pink dataset spanned a limited ge-
 129 ographical (tropical–subtropical Atlantic) and temperature (25–28°C) range, complicat-
 130 ing accurate determination of regression coefficients. Likewise, *N. pachyderma* and *N.*
 131 *incompta* were combined and calibrated together as the *N. pachyderma* group. Origin-
 132 ally considered to be morphotypes, *N. pachyderma* and *N. incompta* are now classified
 133 as genetically different species (Darling et al., 2006) and have different temperature opti-
 134 ma (which is accounted for in our seasonal calibration). However, they have similar habi-
 135 tat preferences, living seasonally in the high latitudes in the mixed layer (Darling et al.,
 136 2006), and as with *G. ruber* pink, we found that the limited number of *N. pachyderma*
 137 core tops challenged calibration in isolation.

138 The core top data are matched to the nearest gridpoint from the World Ocean At-
 139 las 2013 (WOA13) version 2 (Boyer et al., 2013), from which we draw mean annual and
 140 seasonal SSTs and sea-surface salinity (SSS). As with our previous calibration models
 141 for foraminiferal $\delta^{18}\text{O}$ (Malevich et al., 2019), we do not explicitly consider depth habi-
 142 tat for the different planktic groups. Although regressing against environmental param-
 143 eters at 0 m water depth might not be optimal to derive the ‘true’ sensitivities of Mg/Ca,
 144 we assume that users want to infer past SSTs from mixed-layer species, rather than a
 145 calcification depth temperature. In addition, depth preferences tend to co-vary with sea-
 146 sonal preferences and so accounting for both can lead to overfitting. We tested this as-
 147 sumption by running our Bayesian calibration models using integrated 0–50m values; we
 148 obtained nearly identical coefficients (not shown). We note that any prescribed depth
 149 habitat in a calibration – whether it be 0 m or 0–50m – assumes that it is static in time.
 150 Circumventing this assumption requires modeling depth habitat explicitly as a function
 151 of thermal tolerance, light, and nutrients (e.g., Lombard et al., 2011). This adds consid-
 152 erable complexity, and paleoclimate applications would require biogeochemical constraints,
 153 thus we leave this for future work.

154 Seasonal averages are computed using spatially-varying estimates of when the peak
 155 abundance of each foraminiferal species occurs, according to their individual thermal tol-
 156 erances. As described in Malevich et al. (2019), these are based on kernel density esti-
 157 mates (KDE) of sediment trap data (Žarić et al., 2005) and the seasonal cycle in tem-
 158 perature at each site, as inferred from WOA13. For example, the KDE of *G. ruber* abun-
 159 dance indicates that this species prefers SSTs between 22.5 and 31.9 °C. Thus, for lo-
 160 cations with SSTs that seasonally drop below 22.5°C, *G. ruber* is assumed to not calcify
 161 during those months, and the average seasonal SST would be the mean value for all
 162 months above 22.5°C. Effectively, this assumes that *G. ruber* Mg/Ca reflects mean an-
 163 nual SSTs at most tropical locations, but warm-season SSTs in the subtropics. We also
 164 draw seasonal optima for *N. pachyderma* and *N. incompta* separately, recognizing the
 165 distinct temperature preferences of these two species, even though they are ultimately
 166 calibrated together. Table 1 lists the minimum, maximum, and median SST preferences

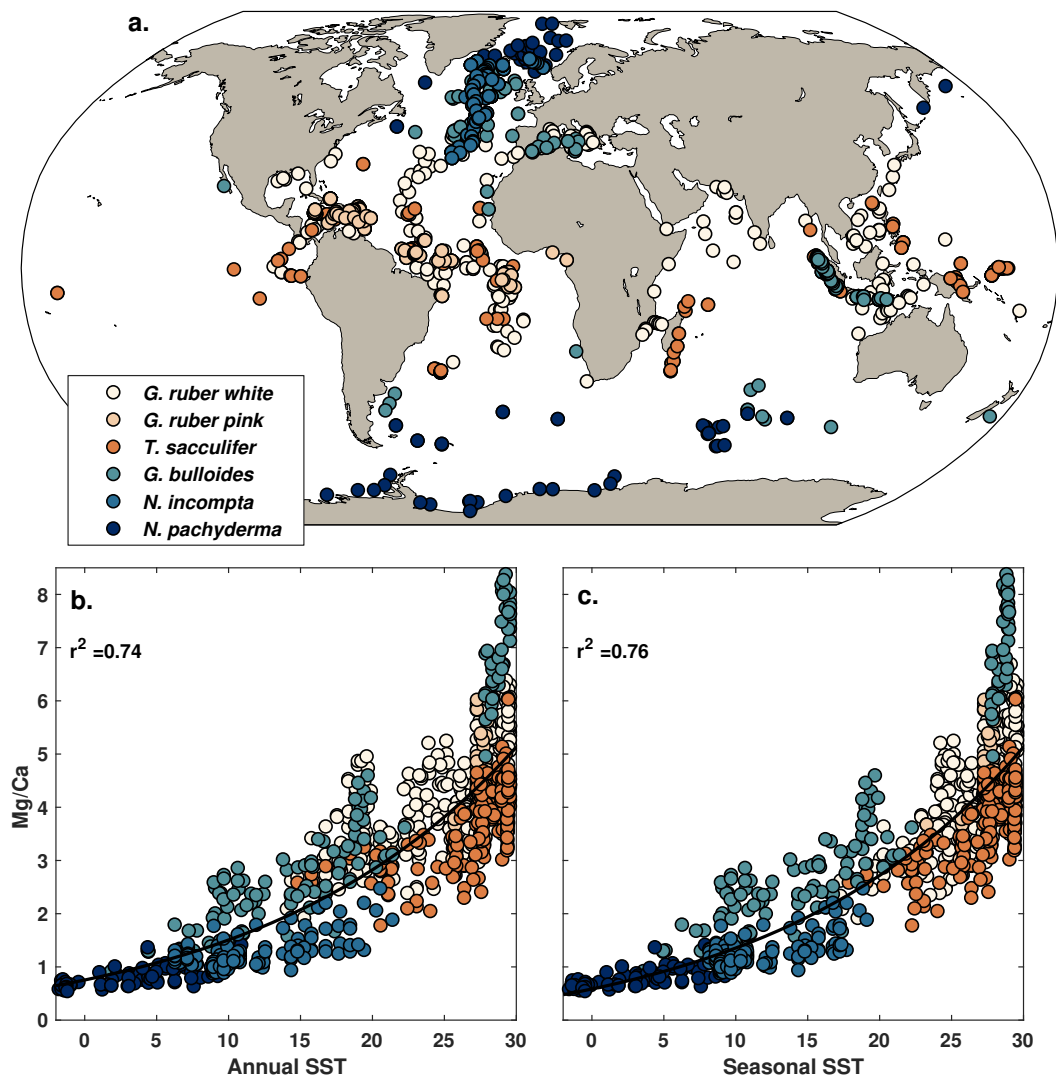


Figure 1. a. Geographical distribution of the Mg/Ca core top data, with an “include” flag of 1 ($N = 1153$), by species. b. The relationship between Mg/Ca and mean annual SSTs. c. The relationship between Mg/Ca and estimated seasonal SSTs. Black lines through the data in (b.) and (c.) represent the best-fit exponential regressions, with r^2 values listed in the upper left.

167 for each species according to the KDE method. For *G. ruber*, *T. sacculifer*, and *N. incompta*,
 168 our inferred optimal SST ranges are very similar to those modeled by Lombard
 169 et al. (2009) from culture data (21–30°C; 19–31°C; 6–20°C; respectively). Our ranges
 170 for *G. bulloides* and *N. pachyderma* are slightly larger (Table 1) than the Lombard et
 171 al. (2009) estimates (10–25°C; 0–10°C; respectively) because the sediment trap data indicate
 172 a wider thermal range for these species.

173 Core tops that fall within the same gridpoint, and contain the same species, are
 174 further averaged prior to calibration exercises to reduce the impact of spatial clustering
 175 on the regression parameters. This results in an effective core top N of 690 for our regression
 176 models, with $N = 330$ for *G. ruber*, $N = 141$ for *T. sacculifer*, $N = 100$ for
 177 *G. bulloides* model, and $N = 119$ for *N. pachyderma*.

Table 1. Sea-surface temperature ranges associated with peak abundances for each foraminiferal species investigated in this study, based on kernel density estimates of shell fluxes from a collection of global sediment traps (from Malevich et al., 2019)

Species	Peak Abundance SST ranges ($^{\circ}\text{C}$)		
	Min	Max	Median
<i>G. ruber</i>	22.5	31.9	27.4
<i>T. sacculifer</i>	20.2	30.6	27.0
<i>G. bulloides</i>	3.6	29.2	18.0
<i>N. pachyderma</i>	-0.9	15.3	5.4
<i>N. incompta</i>	6.7	21.1	15.3

178 Since previous work indicates that the carbonate system influences foraminiferal
 179 Mg/Ca, we also collate surface water pH and bottom water calcite saturation state (Ω)
 180 values for each core site from the Global Ocean Data Analysis Project (GLODAP) ver-
 181 sion 2 gridded climatology (Lauvset et al., 2016). GLODAPv2 lacks coverage in the Gulf
 182 of Mexico, so for core tops in this location we rely on bottle data collected as part of the
 183 second Gulf of Mexico and East Coast Carbon Cruise (GOMECC-2) in 2012 (data pub-
 184 licly available from <http://www.aoml.noaa.gov/ocd/gcc/GOMECC2>) and use the MAT-
 185 LAB implementation of CO2SYS (v1.1, Van Heuven et al., 2011) to compute pH and
 186 calcite Ω from measured values of alkalinity, dissolved inorganic carbon, salinity, tem-
 187 perature, pressure, silicate, and phosphate.

188 Overall, our core top dataset spans a wide range of SSTs (-1.6 to 29.6 $^{\circ}\text{C}$; 95% CI
 189 = 1.1 to 29.4 $^{\circ}\text{C}$) and Ω (0.7 to 5.6; 95% CI = 0.9 to 4.1). Although high and low SSS
 190 values are represented in the dataset (28.4 to 39.3 psu), the distribution of the data is
 191 more restricted (95% CI = 33.3 to 38.4 psu). The range of surface water pH values sam-
 192 pled is limited (7.91 to 8.23; 95% CI = 8.01–8.18), reflecting the fact that the pH of the
 193 modern surface ocean does not have a large dynamic range.

194 As described below, we also use Mg/Ca data from cultured foraminifera to con-
 195 strain sensitivities to environmental parameters. We use the compilation of Gray and
 196 Evans (2019), with the addition of the *G. ruber* pink data from Allen et al. (2016) and
 197 *N. incompta* data from Von Langen et al. (2005) and Davis et al. (2017). This updated
 198 culture dataset includes 30 *G. ruber* observations, 20 *T. sacculifer* observations, 12 *G.*
 199 *bulloides* observations, 29 *O. universa* observations and 12 *N. incompta* observations for
 200 a total of 103 data points.

201 3 Model form and exploration of environmental predictors

202 Temperature clearly exerts a strong, non-linear control on core top Mg/Ca, explain-
 203 ing about 75% of the variance in the data (Fig. 1b,c), in agreement with experimental
 204 evidence (e.g., Lea et al., 1999). However, laboratory studies and previous core top in-
 205 vestigations have shown that pH, salinity, the saturation state (Ω) at the core site, the
 206 cleaning method, and shell size also influence Mg/Ca. Mg/Ca sensitivities to salinity and
 207 pH are also considered exponential (Lea et al., 1999; Kisakürek et al., 2008; Hönisch et
 208 al., 2013; Evans, Wade, et al., 2016; Gray et al., 2018). Culture experiments suggest a
 209 pH sensitivity of -50 to -90% per pH units for *O. universa*, *G. bulloides*, and *G. ruber*
 210 (white) (Lea et al., 1999; Russell et al., 2004; Kisakürek et al., 2008; Evans, Brierley, et
 211 al., 2016; Gray & Evans, 2019), and Gray et al. (2018) detected a pH sensitivity of a sim-
 212 ilar magnitude of -80% \pm 70% (2σ) per pH units in a global compilation of *G. ruber* (white)
 213 sediment trap data. However, pH does not seem to impact Mg/Ca in cultures of *N. pachy-*
 214 *derma*, *N. incompta* (Davis et al., 2017) and *T. sacculifer* (Allen et al., 2016). Labora-

215 tory experiments indicate a moderate sensitivity of planktic Mg/Ca to salinity (3–5%
 216 per psu) (Lea et al., 1999; Kısakürek et al., 2008; Hönisch et al., 2013; Allen et al., 2016;
 217 Gray & Evans, 2019). Previous core top studies suggested a much larger sensitivity (15–
 218 59%, Ferguson et al., 2008; Mathien-Blard & Bassinot, 2009; J. Arbuszewski et al., 2010)
 219 but reanalyses indicated that these high estimates are due to environmental co-variates
 220 (Hertzberg & Schmidt, 2013; Hönisch et al., 2013; Khider et al., 2015). Core top obser-
 221 vations also reveal a systematic decline in sedimentary planktic Mg/Ca – regardless of
 222 species – under low bottom water calcite saturation state at the site of deposition (Regenberg
 223 et al., 2014). Finally, intra- and inter-laboratory comparisons (Barker et al., 2003; Rosen-
 224 thal et al., 2004) as well as a regression analysis of *G. ruber* (white) core tops (Khider
 225 et al., 2015) indicate a systematic offset in measured Mg/Ca of ~10-15% based on whether
 226 the laboratory cleaning method includes a reductive step. Mg/Ca also varies by shell size
 227 (Elderfield et al., 2002; Friedrich et al., 2012), but researchers tend to mitigate this ef-
 228 fect by picking foraminifera from a restricted size fraction. As discussed below, we do
 229 not detect a significant influence of shell size on our core top Mg/Ca data, so it is not
 230 included in our model form.

231 Since temperature, salinity, and pH sensitivities are exponential, we transform Mg/Ca
 232 to $\ln(\text{Mg/Ca})$ for model fitting. This transformation also assumes that the errors for a
 233 Mg/Ca model follow an exponential distribution; the data in Figure 1b and 1c suggest
 234 that this is a valid assumption, as variance increases non-linearly with temperature. Fol-
 235 lowing Khider et al. (2015), the cleaning parameter acts as a multiplicative term in Mg/Ca
 236 space, and thus an additive term in $\ln(\text{Mg/Ca})$ space, with the understanding that re-
 237 ductive cleaning (a value of 1) results in a systematic decline in Mg/Ca. The form of the
 238 Mg/Ca dependency on Ω is less clear. Regenberg et al. (2014) and Khider et al. (2015)
 239 assume that bottom water saturation impacts Mg/Ca of tests linearly below a certain
 240 threshold, which they define based on ΔCO_3^{2-} instead of Ω . These two quantities are
 241 functionally equivalent, but we prefer using Ω because it is always a positive value. How-
 242 ever, it might be expected, based on reaction kinetics, that Mg/Ca should have a non-
 243 linear dependency on saturation state, with dissolution increasing as saturation state drops
 244 (Sjöberg, 1976). Indeed, if we remove the impact of SST on our pooled dataset, we find
 245 that $\ln(\text{Mg/Ca})$ residuals trend non-linearly with Ω , with the slope becoming steeper as
 246 Ω becomes smaller (Fig. 2). The relationship is strongest below an Ω of ~ 1.5 (Fig. 2),
 247 which is consistent with the ΔCO_3^{2-} threshold of ~ 40 $\mu\text{mol/kg}$ identified by Regenberg
 248 et al. (2014). Ω sensitivity can be approximated by a power function, with a coefficient
 249 of -2 (Fig. 2). This supports a transformation of Ω to Ω^{-2} in order to linearize the sen-
 250 sitivity of $\ln(\text{Mg/Ca})$ to saturation state.

251 The final form of a core top Mg/Ca forward model, based on the physical expect-
 252 ations outlined above, is:

$$253 \quad \ln(\text{Mg/Ca}) = \alpha + \mathbf{T} \cdot \beta_T + \mathbf{S} \cdot \beta_S + \mathbf{pH} \cdot \beta_P + \mathbf{\Omega}^{-2} \cdot \beta_O + (1 - \mathbf{clean} \cdot \beta_C) + \epsilon, \quad (1)$$

$$254 \quad \epsilon \sim \mathcal{N}(\mathbf{0}, \sigma^2)$$

255 where ϵ is the vector of residual errors, approximated by a Normal distribution with mean
 256 zero and variance σ^2 .

257 To assess the impact of each environmental variable on model performance, we it-
 258 iteratively computed regressions using ordinary least squares, adding each predictor se-
 259 quentially. We then compared the Bayesian Information Criterion (BIC) for each iter-
 260 ative model to determine whether the additional predictor resulted in improvement. We
 261 also analyzed the significance of each predictor’s coefficient. We do this for both the pooled
 262 dataset (using annual and seasonal SST and SSS estimates) and the four species groups
 263 (using seasonal SST and SSS estimates), and discuss the results for each predictor in turn.

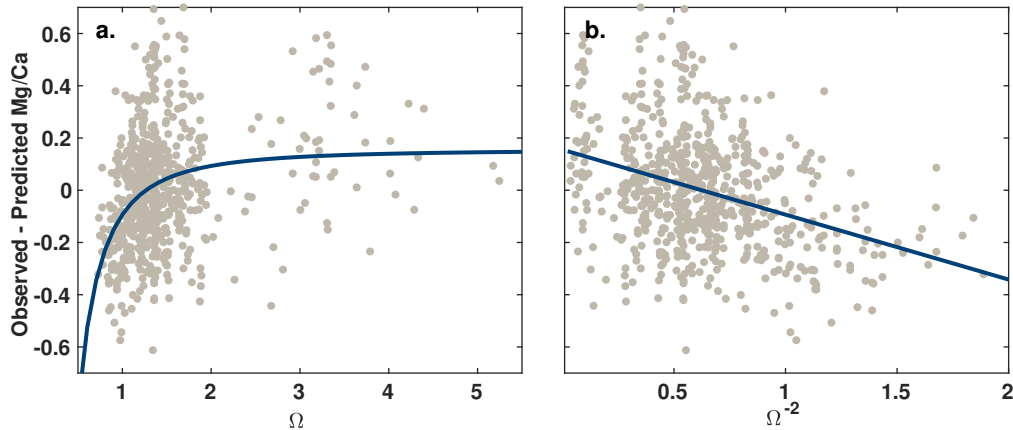


Figure 2. The relationship of core top $\ln(\text{Mg}/\text{Ca})$ residuals (observed-predicted; all species; $N = 690$) to a. bottom water calcite Ω and b. Ω^{-2} after removing the dependence on temperature. Dots represent individual core tops; lines show the best fit regression.

264

3.1 Temperature

265

266

267

268

269

270

271

272

273

274

275

276

277

278

For both the pooled annual and pooled seasonal datasets, we find that SST alone explains over 80% of the variance in $\ln(\text{Mg}/\text{Ca})$ (Table 2). This is slightly greater than an exponential model for Mg/Ca (Fig. 1b and c), reflecting some improvement in the fit associated with the assumption that variance increases exponentially. Temperature remains the most important parameter for the individual species models, although, it explains only ca. 50% of the variance for the warm-water groups (*G. ruber* and *T. sacculifer*; Table 2). This is due to the relatively restricted temperature ranges for *G. ruber* and *T. sacculifer* (ca. 12°C) compared to those for *G. bulloides* and *N. pachyderma* (> 20°C), which allows for more variance to be explained by the other environmental factors. The temperature sensitivity is similar across all species, between 5–7% (Table 2). This agrees well with recent re-assessments from culture and sediment traps, both of which indicate a temperature sensitivity of ca. 6% (Gray et al., 2018; Gray & Evans, 2019) rather than 9%, as previously assumed (e.g., Dekens et al., 2002; Anand et al., 2003; Khider et al., 2015).

279

3.2 Bottom water calcite saturation (Ω)

280

281

282

283

284

285

286

287

288

289

290

291

292

293

The addition of Ω as a predictor improves almost all of the models (r^2 increases, RMSE decreases, and BIC decreases), with the biggest impact on the warm-water species (Table 2). The large drop in BIC associated with the addition of this parameter (to the pooled models in particular, where it is about 100) supports long-standing theory and intuition that inclusion of Ω improves prediction of core top Mg/Ca (Rosenthal & Boyle, 1993; Russell et al., 1994; Brown & Elderfield, 1996; Rosenthal et al., 2000; Dekens et al., 2002; Regenberg et al., 2014). Ω sensitivity remains fairly constant across species groups, in agreement with previous work that most species of planktic foraminifera are sensitive to saturation state at the site of deposition (Regenberg et al., 2014). The possible exception is the *N. pachyderma* group, for which Ω is not a significant predictor (Table 2). Ω ranges between 0.7 and 2.8 within this group, hence the lack of sensitivity does not reflect a limitation of the data. It may be that *N. pachyderma* and *N. incompta* are indeed less sensitive to dissolution, in agreement with buoy exposure experiments (Berger, 1970), although the error on the Ω coefficient is large ($\pm 0.1, 2\sigma$).

Table 2. Regression model metrics and coefficients. RMSE = root mean square error (in $\ln(\text{Mg}/\text{Ca})$ units). Each column notes the addition (or subtraction) of a predictor relative to the column to the left. Group-specific models were calculated with seasonal temperature and salinity estimates. BIC = Bayesian Information Criterion. Lower values indicate improved performance. n denotes the number of core tops (after gridding, see Section 2). Coefficients correspond to that of the added predictor. Coefficients in italics are not significantly different than zero (at $p = 0.05$).

	SST	+ Ω^{-2}	+ clean	+ SSS	-SSS +pH
<i>Pooled annual, n = 690</i>					
r^2	0.83	0.86	0.87	0.88	0.87
RMSE	0.24	0.22	0.21	0.20	0.21
BIC	13	-114	-172	-213	-167
Coefficient	0.063	-0.33	0.15	0.049	<i>0.16</i>
<i>Pooled seasonal, n = 690</i>					
r^2	0.86	0.88	0.89	0.89	0.89
RMSE	0.22	0.21	0.20	0.20	0.20
BIC	-112	-202	-277	-276	-272
Coefficient	0.055	-0.26	0.16	0.015	<i>0.28</i>
<i>G. ruber n = 330</i>					
r^2	0.48	0.60	0.63	0.63	0.63
RMSE	0.15	0.13	0.13	0.13	0.13
BIC	-313	-387	-407	-405	-405
Coefficient	0.062	-0.22	0.075	<i>0.011</i>	<i>0.48</i>
<i>T. sacculifer, n = 141</i>					
r^2	0.47	0.69	0.79	0.79	0.81
RMSE	0.14	0.11	0.09	0.09	0.08
BIC	-154	-224	-275	-274	-288
Coefficient	0.054	-0.27	0.14	0.018	1.3
<i>G. bulloides, n = 100</i>					
r^2	0.86	0.88	0.88	0.89	0.89
RMSE	0.19	0.17	0.17	0.17	0.17
BIC	-44	-60	-57	-54	-55
Coefficient	0.068	-0.29	<i>0.12</i>	<i>-0.024</i>	<i>-1.0</i>
<i>N. pachyderma, n = 119</i>					
r^2	0.78	0.79	0.80	0.80	0.80
RMSE	0.15	0.15	0.15	0.15	0.15
BIC	-109	-107	-108	-106	-106
Coefficient	0.052	<i>-0.06</i>	0.088	<i>0.047</i>	<i>0.57</i>

294

3.3 Cleaning

295

296

297

298

299

300

The addition of the cleaning parameter improves the statistics for the pooled models and the warm-water groups, with drops in BIC on the order to 10–50 (Table 2) but has little impact on *G. bulloides* and *N. pachyderma*. In the case of *G. bulloides*, this reflects a limitation of the data subset: all but two of the core tops were cleaned with the oxidative protocol, so it is not possible to reliably detect the influence of reductive cleaning. For *N. pachyderma*, the influence of cleaning on model skill is small but the

301 derived coefficient (9%) is very close to the other species (8-14%), and is in agreement
 302 with previous estimates (Barker et al., 2003; Rosenthal et al., 2004; Khider et al., 2015).
 303 Overall, the change in BIC suggests that inclusion of laboratory cleaning does notably
 304 improve prediction of core top Mg/Ca and, the limitation of the *G. bulloides* data sub-
 305 set aside, the sensitivity should be relatively consistent across species, as expected from
 306 laboratory investigations (Barker et al., 2003).

307 3.4 Salinity

308 The addition of salinity to the model does not significantly improve the statistics
 309 for the species group regressions, nor for the pooled seasonal model (BIC is mostly un-
 310 changed; Table 2). The inferred sensitivity to salinity is low or statistically insignificant
 311 in all of these cases (ca. 2% per psu). There is however improvement in the pooled an-
 312 nual model (BIC drops by 40) and the inferred sensitivity is higher (4.9% per psu). The
 313 inferred sensitivity in the pooled seasonal model of $1.5 \pm 1.4\%$ (2σ) is lower than (al-
 314 though technically still consistent with) the best estimate from culture studies ($3.6 \pm$
 315 1.2% , 2σ ; Gray & Evans, 2019), whereas the pooled annual value falls on the higher end
 316 of culture-based expectations. Overall, these results suggest that the addition of salin-
 317 ity neither improves nor degrades core top Mg/Ca prediction, and furthermore that the
 318 magnitude of the salinity sensitivity is difficult to compute from the core top dataset.
 319 Although there can be strong salinity gradients in the surface ocean, this result is not
 320 due to our choice to calibrate to surface salinity; derived sensitivities from 0–50 m av-
 321 erage values yield equally low values (not shown). Rather, the accuracy of the derived
 322 salinity sensitivities is restricted by both the limited range of values in our core top dataset
 323 (95% CI = 33.3 to 38.4 psu), and the strong covariation between temperature and salin-
 324 ity that is typical of global ocean. Since the high latitudes are fresh and cold, and the
 325 subtropics warm and salty, below SSTs of 21°C, SST and SSS are positively correlated
 326 in our dataset ($\rho = 0.87, p < 0.0001$). Since the tropics are warm and fresh, above 21°C
 327 SST and SSS are negatively correlated ($\rho = -0.73, p < 0.0001$). Even though the di-
 328 rection of the correlation flips, this high degree of relation creates a condition of collinear-
 329 ity, especially for the group data subsets as they fall on one side of the relationship or
 330 the other (except for *G. bulloides*). This means that the OLS-derived coefficients for SSS
 331 are not readily interpretable.

332 3.5 pH

333 The addition of pH degrades model performance and/or yields insignificant or un-
 334 realistic coefficients (Table 2). The expected sensitivity from laboratory experiments is
 335 $-70 \pm 14\%$ per pH unit; in comparison, our coefficients are generally of the incorrect sign
 336 (Table 2). This is unsurprising given the restricted range of values (8.01–8.18, 95% CI)
 337 in our dataset, and more broadly, in the modern ocean. In addition, pH is collinear with
 338 temperature ($r = -0.70, p < 0.0001$), because cold locations have a higher pH. It is
 339 also possible that the water column pH observations derived from the GLODAPv2 prod-
 340 uct are inaccurate. Point GLODAP measurements from the upper water column may
 341 not fully sample seasonal and year-to-year variability, and include the impact of anthro-
 342 pogenic CO₂, which, in most locations, would not be represented in core top Mg/Ca val-
 343 ues. Overall, this demonstrates that Mg/Ca sensitivity to pH cannot be reliably recov-
 344 ered from core top data, mainly due to the limitations of the observations and covari-
 345 ation with temperature.

346 3.6 Shell size

347 Size fractions were not available for all core tops in our dataset, so statistics for a
 348 shell size predictor cannot be compared directly to those for full core top data (Ta-
 349 ble 2). However, analysis of the subset of data that do contain this information indicates

350 that size fraction is not a significant predictor for core top Mg/Ca, for any species group
 351 (not shown). In contrast with a recent core top calibration study (Saenger & Evans, 2019),
 352 we did not detect a significant sensitivity to shell size for the *N. pachyderma* group. This
 353 may reflect differences in respective choices of the depth and seasonality of temperatures
 354 to calibrate to, and/or differences in the metrics used to determine if an environmental
 355 factor is a significant predictor. Either way, the implication is that size fraction is not
 356 a strong predictor of core top Mg/Ca, in agreement with previous analysis of sediment
 357 trap data (Gray et al., 2018). As noted above, this may in part reflect pre-emptive size
 358 restriction of behalf of the analysts. We thus do not consider size fraction in formulat-
 359 ing forward or inverse models.

360 3.7 Summary of environmental sensitivities

361 Our iterative regression analysis identifies temperature, Ω , and the laboratory clean-
 362 ing method as significant predictors of core top Mg/Ca. Salinity is a weak predictor, but
 363 derived sensitivities may be inaccurate due to covariation with temperature. The pH sen-
 364 sitivity cannot be recovered at all due to covariation and inaccuracies in the core top dataset.
 365 From an empirical point of view, these findings support the omission of salinity and pH
 366 from the Mg/Ca model. However, it is well-known from culture studies that salinity and
 367 pH are important influences on Mg/Ca, and can bias estimates of past temperatures (Khider
 368 et al., 2015; Gray & Evans, 2019). We therefore retain these predictors, but in order to
 369 provide better constraints on their coefficients, we develop Bayesian hierarchical mod-
 370 els in which both the culture and core top data are used to constrain parameters. This
 371 model structure leverages in the information in both the experimental (laboratory) data
 372 and the empirical (core top) data, ultimately allowing for more accurate prediction of
 373 Mg/Ca.

374 4 BAYMAG: a Bayesian calibration model for Mg/Ca

375 4.1 Model design

376 Following our previous work with $\delta^{18}\text{O}$ of foraminifera (Malevich et al., 2019), we
 377 developed two styles of forward models to represent core top Mg/Ca: one that pools all
 378 core top data together (mainly for deep-time applications with non-extant species) and
 379 another that treats each species group separately, with information shared through pa-
 380 rameters and hyperparameters. The models are hierarchical, leveraging both culture and
 381 core top Mg/Ca data. The pooled model design is:

$$382 \ln(\text{Mg/Ca}_c) = \begin{cases} \alpha_i + \mathbf{T}_c \cdot \beta_{T_c} + \mathbf{S}_c \cdot \beta_S + \epsilon_c & \text{if } \textit{incompta, sacculifer} \\ \alpha_i + \mathbf{T}_c \cdot \beta_{T_c} + \mathbf{S}_c \cdot \beta_S + \mathbf{pH}_c \cdot \beta_P + \epsilon_c & \text{if } \textit{ruber, bulloides, universa} \end{cases} \quad (2)$$

$$\epsilon_c \sim \mathcal{N}(\mathbf{0}, \sigma_{ci}^2)$$

$$383 \ln(\text{Mg/Ca}) = \alpha + \mathbf{T} \cdot \beta_T + \mathbf{S} \cdot \beta_S + \mathbf{pH} \cdot \beta_P + \Omega^{-2} \cdot \beta_O + (1 - \mathbf{clean} \cdot \beta_C) + \epsilon, \quad (3)$$

$$\epsilon \sim \mathcal{N}(\mathbf{0}, \sigma^2)$$

384 with different values of α and σ for each i cultured species. Hyperparameters on the cul-
 385 ture temperature coefficient are:

$$386 \beta_{T_c} \sim \mathcal{N}(\mu_{\beta T}, \sigma_{\beta T}^2) \quad (4)$$

387 and the culture temperature coefficient acts as a prior on the core top temperature co-
 388 efficient:

$$\beta_T \sim \mathcal{N}(\beta_{T_c}, \sigma_{\beta T}^2) \quad (5)$$

389 The top of the model hierarchy (Eq. 2) describes Mg/Ca in the culture dataset (see Sec-
 390 tion 2 for a description of the data compilation) and accounts for the fact that Mg/Ca
 391 in cultures of *N. incompta* and *T. sacculifer* is not sensitive to pH (Allen et al., 2016;
 392 Davis et al., 2017). Otherwise, the temperature, salinity, and pH sensitivities are assumed
 393 to be similar across cultured species, while the intercept and error terms are allow vary
 394 between each species i to account for offsets in the mean and variance of $\ln(\text{Mg}/\text{Ca})$. As
 395 a reality check, we run this top part of the model independently to assess how well it pre-
 396 dicted culture Mg/Ca data alone. We find that this top hierarchy yields excellent predic-
 397 tion and the posterior coefficients for temperature, salinity, and pH are similar to pre-
 398 vious assessments done with an ordinary least squares approach (Gray & Evans, 2019)
 (Fig. 3), validating our model design.

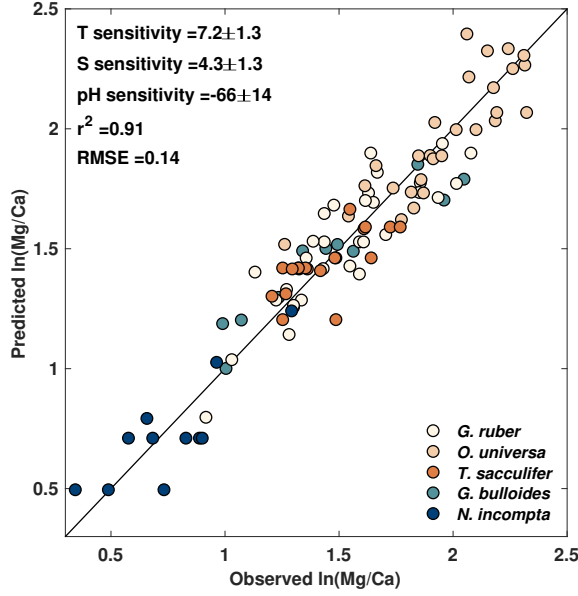


Figure 3. Bayesian hierarchical model results for planktic Mg/Ca culture data, including median and 2σ ranges for the posterior temperature, salinity, and pH sensitivities.

399

400 The lower part of the hierarchy (Eq. 3) contains the model for the core top data.
 401 Since the core tops are pooled together across all species, it assumes a generic pH sen-
 402 sitivity. The pH and salinity sensitivities (β_P and β_S) are constrained by the culture data
 403 in the top part of the hierarchy, and then allowed to influence the core top data. Con-
 404 versely, the sensitivities to Ω and the cleaning method (β_O and β_C) are only constrained
 405 by the core top data. The temperature sensitivities β_{T_c} and β_T are constrained by both
 406 the culture and core top data, with the former acting as the prior mean for the latter.

407

The group-specific core top model takes the slightly modified form,

$$\ln(\text{Mg}/\text{Ca}_c) = \begin{cases} \alpha_i + \mathbf{T}_c \cdot \beta_{T_c} + \mathbf{S}_c \cdot \beta_S + \epsilon_c & \text{if } \textit{incompta}, \textit{sacculifer} \\ \alpha_i + \mathbf{T}_c \cdot \beta_{T_c} + \mathbf{S}_c \cdot \beta_S + \mathbf{pH}_c \cdot \beta_P + \epsilon_c & \text{if } \textit{ruber}, \textit{bulloides}, \textit{universa} \end{cases} \quad (6)$$

$$\epsilon_c \sim \mathcal{N}(\mathbf{0}, \sigma_{ci}^2)$$

408

$$\ln(\text{Mg/Ca}) = \begin{cases} \alpha_j + \mathbf{T} \cdot \beta_T + \mathbf{S} \cdot \beta_S + \Omega^{-2} \cdot \beta_O + (1 - \mathbf{clean} \cdot \beta_C) + \epsilon & \text{if } \textit{pachy}, \textit{sacculifer} \\ \alpha_j + \mathbf{T} \cdot \beta_T + \mathbf{S} \cdot \beta_S + \mathbf{pH} \cdot \beta_P + \Omega^{-2} \cdot \beta_O + (1 - \mathbf{clean} \cdot \beta_C) + \epsilon & \text{if } \textit{ruber}, \textit{bulloides} \end{cases} \quad (7)$$

$$\epsilon \sim \mathcal{N}(\mathbf{0}, \sigma_i^2)$$

409 with hyperparameters and priors on the temperature coefficients as above (Eqs. 4 and
 410 5). The top part of the hierarchy (Eq. 6), describing the culture data, is identical to the
 411 pooled model (Eq. 2). The lower part of the hierarchy (Eq. 7) describes the core top data,
 412 and since species are treated independently, accounts for the fact that the *T. sacculifer*
 413 and *N. pachyderma* core tops should not be sensitive to pH. As with the culture data,
 414 the intercept and error terms (α_j and σ_j) are allowed to vary for each j foraminiferal
 415 species. The temperature, salinity, Ω and cleaning sensitivities are computed across all
 416 of the data and are not allowed to vary by species. This choice was made because our
 417 regression experiments indicated that, with few exceptions, these sensitivities are sim-
 418 ilar across species (Table 2). Although we did observe a lower Ω sensitivity for the *N.*
 419 *pachyderma* group (see Section 3.2), computation of a hierarchical model with group-
 420 specific Ω coefficients yielded no improvement in model skill. Likewise, computation of
 421 group-specific temperature coefficients did not improve skill, supporting our assumption
 422 (and inferences from the culture data) that temperature sensitivity should be similar across
 423 species.

424 For all models, we estimate parameters using Bayesian inference and Markov chain
 425 Monte Carlo sampling (Gelman et al., 2003) with Stan software, version 2.19.0 (Carpenter
 426 et al., 2017). Priors for the parameters and hyperparameters, as well as prior vs. pos-
 427 terior plots, are given in Appendix A. To assess the impact of using annual vs. seasonal
 428 SST and SSS, we computed the pooled and group-specific models with both sets of val-
 429 ues, although we recommend use of either the pooled annual or group-specific seasonal
 430 models for practical applications. We perform Pareto-Smoothed Importance Sampling
 431 Leave-One-Out (psis-loo) cross-validation to compare predictive accuracy between mod-
 432 els (Vehtari et al., 2017). These values are reported as expected log pointwise predictive
 433 density (elpd); larger values indicate a better fit to the data.

434 4.2 Model results

435 The pooled annual model explains 88% of the variance in the core top Mg/Ca data
 436 and has a median root mean square error (RMSE) of 0.20 $\ln(\text{Mg/Ca})$ units (Fig. 4a).
 437 Analysis of the Mg/Ca residuals yields no significant trends with the SST, SSS, Ω , and
 438 cleaning predictors. There is a weak correlation between the residuals and core top pH
 439 (Spearman’s $\rho = 0.13, p = 0.0006$) but as discussed above, we are unsure whether the
 440 core top pH observations are accurate. Likewise, the posterior coefficients for the pH pre-
 441 dictor are very similar to the those derived from the culture data alone (Fig. 3) reflect-
 442 ing limited influence from the core top data. The derived salinity sensitivity is also close
 443 to culture expectations at 4.4%. The median temperature coefficient is lower than the
 444 culture value (6.5 vs. 7.2) although by design, is still the same within uncertainty. This
 445 shift reflects the influence of the core top data, which act to narrow the temperature sen-
 446 sitivity down to a precise estimate of 6.5 ± 0.2 (2σ).

447 While as a whole the residuals are well-distributed across the zero line, there are
 448 systematic offsets according to species (Fig. 4b). This is expected, as neither seasonal-
 449 nor species differences are accounted for in the pooled model. Generally speaking,
 450 the model over-predicts Mg/Ca for *N. pachyderma* and *T. sacculifer* (Fig. 4d and f) and
 451 under-predicts Mg/Ca for *G. ruber* and *G. bulloides* (Fig. 4c and e). These species-level
 452 offsets likely reflect differences in depth habitat. *N. pachyderma* is typically interpreted
 453 to inhabit the upper 100 m of the water column (Reynolds & Thunell, 1986; Elderfield
 454 & Ganssen, 2000; Mortyn & Charles, 2003; Taylor et al., 2018), which would integrate
 455 cooler temperatures than SST and lead to lower observed $\ln(\text{Mg/Ca})$. This may explain

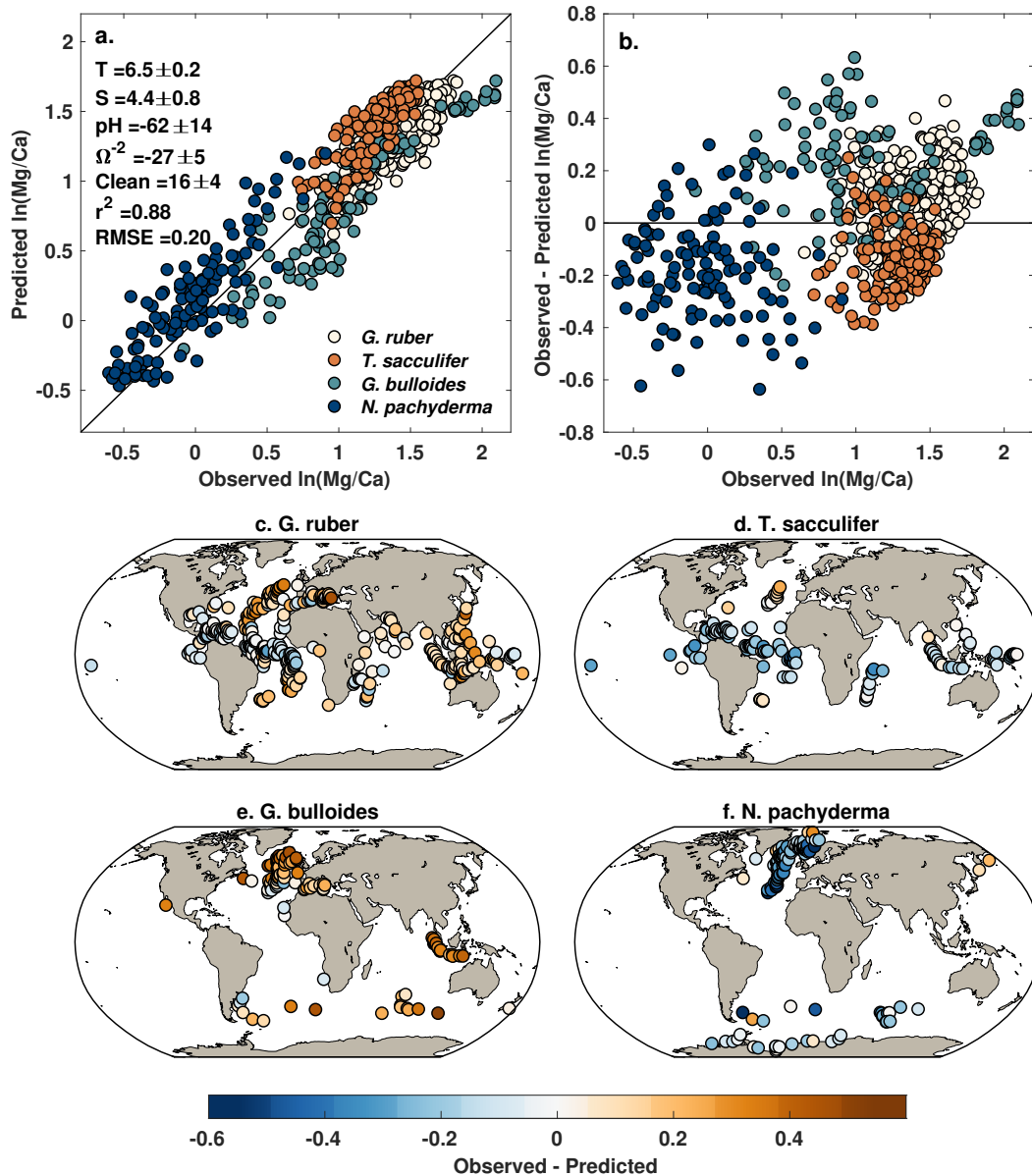


Figure 4. Pooled annual model results. a. Observed vs. predicted $\ln(\text{Mg}/\text{Ca})$, including posterior coefficients for each environmental predictor, colored by species group; b. Model residuals, colored by species group; c.–f. Maps of model residuals for each species group.

456 model overestimation in the high-latitudes (Fig. 4f). Likewise, in the tropics *T. sacculifer*
 457 is often found in a slightly deeper habitat than *G. ruber* (Erez & Honjo, 1981; Fairbanks
 458 et al., 1980; Ravelo & Fairbanks, 1992), leading to lower Mg/Ca than predicted from sur-
 459 face temperatures. This expected offset between *G. ruber* and *T. sacculifer* can be seen
 460 visually in Fig. 4a; at higher values of $\ln(\text{Mg}/\text{Ca})$, *T. sacculifer* plots to the left of *G.*
 461 *ruber*. This explains model over-estimation in the tropics (Fig. 4d). The pooled model
 462 underestimates *G. bulloides* Mg/Ca nearly everywhere, because this species tends to have
 463 higher average Mg/Ca values than *N. pachyderma*, *G. ruber*, and *T. sacculifer* (Elderfield
 464 & Ganssen, 2000; Cléroux et al., 2008) (Fig. 4e).

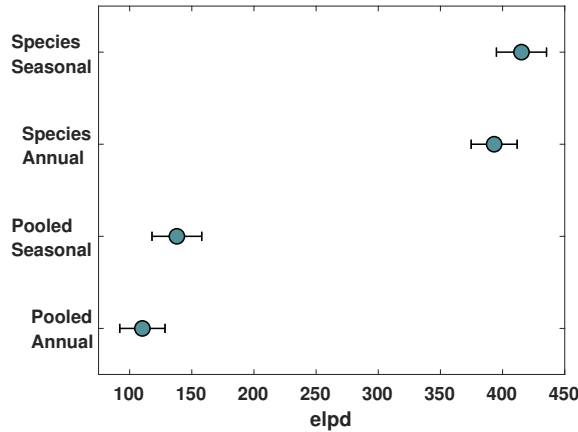


Figure 5. Expected log pointwise predictive density (elpd), based on psis-loo cross validation, for each Bayesian model. Higher values indicate better fit.

465 It is not surprising then that model performance improves markedly with the use
 466 of seasonal SST and SSS and group-specific parameters (Fig. 5). The most significant
 467 improvement comes from implementation of group-specific parameters (Eq. 7), which
 468 cause elpd to rise from 100–150 to ca. 400 (Fig. 5). The seasonal, group-specific model
 469 can account for 95% of the variance in the core top data (Fig. 6) with an RMSE equiv-
 470 alent to that of the culture regression (Fig. 3). The posterior coefficients for tempera-
 471 ture, pH, Ω , and cleaning are similar to the pooled model, and as with the pooled model,
 472 there is no significant correlation between the cleaning and Ω predictors and the resid-
 473 uals and a weak positive correlation with the pH predictor ($\rho = 0.11, p = 0.003$). There
 474 are however weak correlations between the residuals and both temperature and salinity
 475 ($\rho = 0.12, p = 0.001$; $\rho = -0.19, p < 0.0001$). The negative correlation with salinity
 476 is seen in all species groups except *T. sacculifer* and represents the model balance
 477 between the relatively strong salinity sensitivity inferred from the culture data (4.3%,
 478 Fig. 3) and the relatively weak salinity sensitivity that is recovered from the core top
 479 data when seasonal SSTs are used (1.5%, Table 2). As discussed in Section 3.4, the core
 480 top-derived salinity sensitivities are affected by collinearity between SST and SSS, and
 481 therefore may not be accurate. To enforce a sensitivity that is more consistent with the
 482 culture data, we applied an informative prior to the salinity parameter (see Appendix).
 483 The posterior salinity coefficient is still significantly smaller than that of the pooled model
 484 (2.3 ± 0.7 vs. 4.5 ± 1.0) due to core top influence, but is higher than it otherwise would
 485 be without this constraint.

486 The correlation between residuals and temperature seems to be mostly driven by
 487 *G. ruber* residuals, which also show a strong trend with observed $\ln(\text{Mg}/\text{Ca})$ ($r = 0.71, p <$
 488 0.0001). This pattern could arise if the temperature sensitivity for *G. ruber* was system-
 489 atically underestimated; however, the trend is only slightly ameliorated after running a
 490 version of the group-specific model with variable SST coefficients for each species ($r =$
 491 $0.61, p < 0.0001$), and the derived ca. 6% sensitivity of the seasonal group-specific model
 492 is very similar to values calculated from *G. ruber* culture and sediment trap data (Gray
 493 et al., 2018; Gray & Evans, 2019). Alternatively, the pattern could suggest that our rel-
 494 atively simple inference of seasonal SST (based on sediment trap abundances) doesn't
 495 apply well to *G. ruber*. However, we did not see this residual trend in our model for $\delta^{18}\text{O}$
 496 of *G. ruber*, which uses the same seasonal estimation method (Malevich et al., 2019). Ac-
 497 counting for subtle differences in depth habitat would make the trend worse, as studies
 498 suggest that *G. ruber* should have a deeper habitat in the tropics (and therefore lower
 499 Mg/Ca) and shallower one in the subtropics (and therefore higher Mg/Ca) (Hertzberg

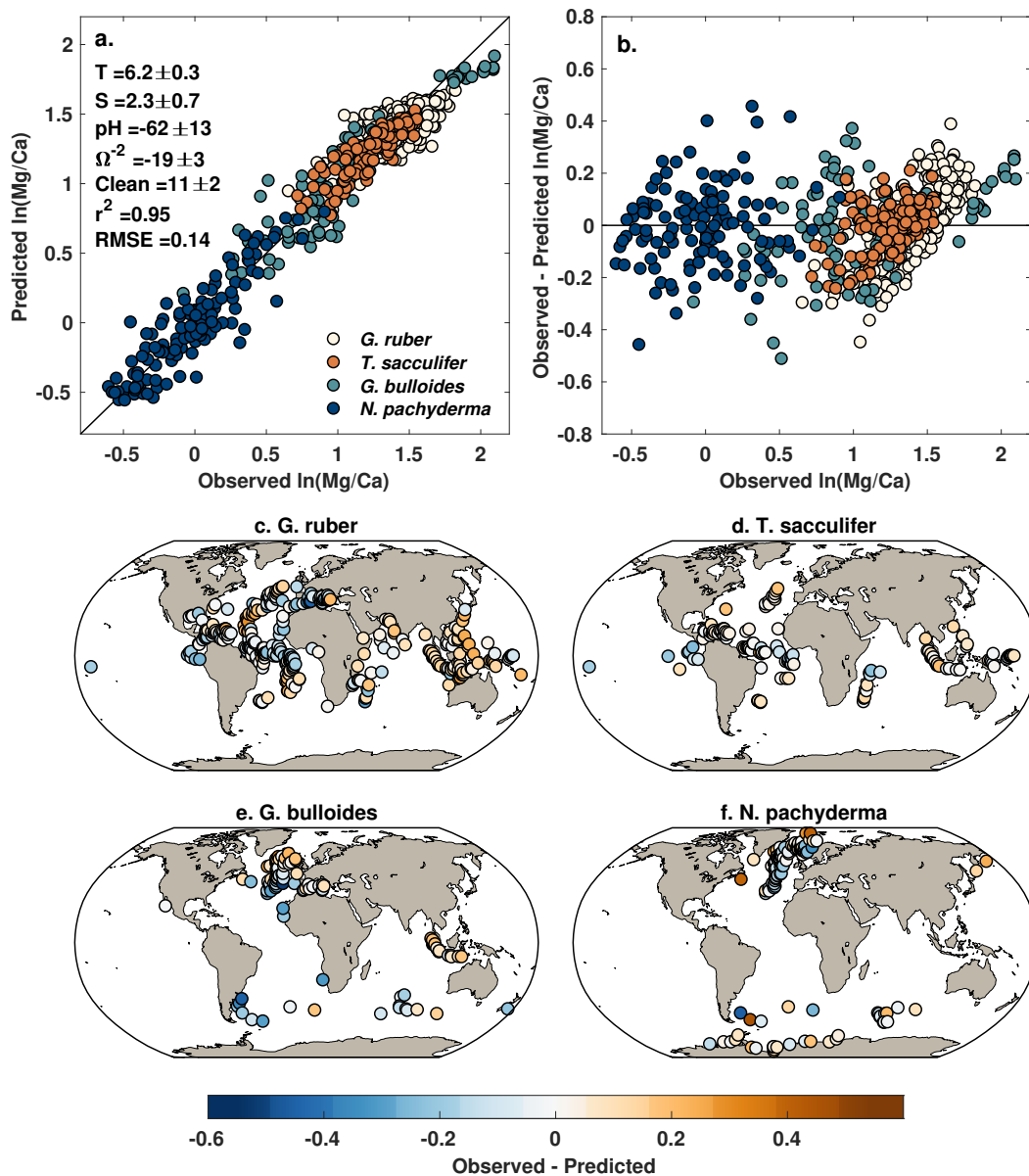


Figure 6. Seasonal, group-specific model results. a. Observed vs. predicted $\ln(\text{Mg}/\text{Ca})$, including posterior coefficients for each environmental predictor, colored by species group; b. Model residuals, colored by species group; c.–f. Maps of model residuals for each species group.

500 & Schmidt, 2013; Hönisch et al., 2013). Similar to *G. ruber*, a group of *G. bulloides* data
 501 with very high Mg/Ca also falls to the right of the one-to-one (Fig. 6). These data
 502 are from the Sumatran margin, where *G. bulloides* calcifies primarily during the cooler
 503 upwelling season, at a depth of ca. 50 m (Mohtadi et al., 2009). This preference should
 504 cause negative, rather than the observed positive, residuals. Taken together, the *G. bul-*
 505 *loides* and *G. ruber* residuals suggest that Mg/Ca sensitivity to temperature may, in fact,
 506 be more non-linear than our model (and all previous exponential models) have assumed,
 507 or alternatively that there is a latent environmental variable or vital effect that scales
 508 non-linearly with temperature. This latent effect is most prominent in *G. ruber* and ac-
 509 counts for the fact that our model can only explain 58% of the variance in *G. ruber* Mg/Ca .

510 Our initial regression experiments likewise demonstrate that only 63% of variance can
 511 be explained using traditional OLS (Table 2). In contrast, our model can explain 78%,
 512 88%, and 77% of the variance in Mg/Ca for *T. sacculifer*, *G. bulloides*, and *N. pachy-*
 513 *derma*, respectively.

514 Further investigation is needed to properly diagnose what this latent variable might
 515 be, but the fact that impacts *G. ruber* and *G. bulloides* preferentially suggests that it
 516 could be pH. pH scales inversely with temperature; warm locations have lower pH and
 517 would be associated with higher Mg/Ca than expected from temperature alone. Although
 518 pH is included in our model, if the GLODAP measurements are inaccurate then this ef-
 519 fect would not be fully accounted for in our Mg/Ca predictions and produce the kind
 520 of residual trends we observe. Indeed, tropical regions, such as the eastern equatorial Pa-
 521 cific and Indo-Pacific warm pool, are poorly observed in the GLODAP dataset, and these
 522 are also locations where the residual error is notably low and high, respectively, for *G.*
 523 *ruber* (Fig. 6c).

524 In spite of the residual trends, the magnitude of the residual bias is still very small
 525 (0.13 ln(Mg/Ca) units, 1σ), and out-of-sample applications of BAYMAG in Section 5
 526 suggest that our model yields good prediction of *G. ruber* Mg/Ca.

527 The seasonal group-specific model eliminates the species-level offsets seen in the
 528 pooled annual model by allowing the intercept terms to vary for each foraminiferal group
 529 (Fig. 6b). These intercept terms effectively compensate for depth habitat preference as
 530 well as any offsets in average Mg/Ca incorporation. Many of the strong spatial trends
 531 in residuals are also minimized (Fig. 6c–f) when compared to the pooled model (Fig. 4c–
 532 f), although some patterns remain. In addition to patterns that may reflect the impact
 533 of the latent variable discussed above, there is a hint of under-prediction in the subtrop-
 534 ical Atlantic and over-prediction in the tropical Atlantic for *G. ruber* (Fig. 6c). The ma-
 535 jority of these points are data from J. Arbuszewski et al. (2010). Hertzberg and Schmidt
 536 (2013) investigated the preservation of *G. ruber* at a few representative sites from the
 537 J. Arbuszewski et al. (2010) dataset and found that, in spite of similar bottom water Ω ,
 538 shells from the subtropics were well-preserved whereas shells from the equatorial sites
 539 were more heavily dissolved. Hertzberg and Schmidt (2013) concluded that overlying high
 540 productivity drove higher levels of respiration in the porewater of the organic-rich sed-
 541 iments from the equatorial sites, leading to enhanced dissolution. This observed pattern
 542 in elevated/degraded foraminiferal preservation, which scales with sedimentary organic
 543 matter as opposed to bottom water Ω , would not be captured by our model and there-
 544 fore would produce the observed residual pattern. For *G. bulloides*, there are negative
 545 residuals in the west African and Benguela upwelling zones; along frontal regions in the
 546 Southern Ocean; and near the confluence of the Brazil and Malvinas currents (Fig. 6e)
 547 indicating that Mg/Ca values are lower than the model predicts. Similar patterns were
 548 observed in the residuals of our Bayesian $\delta^{18}\text{O}$ models (Malevich et al., 2019) and sug-
 549 gest that *G. bulloides* is calcifying during either a cooler season than our seasonal SST
 550 inferences predict, or in a deeper habitat. These patterns could also conceivably reflect
 551 geochemical differences between *G. bulloides* genotypes (Sadekov et al., 2016).

552 5 Application of the BAYMAG forward model

553 BAYMAG can be used to model new values of Mg/Ca (\tilde{y}) from observed or sim-
 554 ulated SST, SSS, pH, Ω , and cleaning protocol by simply drawing from the posterior pre-
 555 dictive distribution, $\tilde{y} \sim \mathcal{N}(\mu, \sigma^2)$, where μ and σ are the core top component of either
 556 the pooled annual or group-specific seasonal model (Eqs. 3, 7). If the user desires, a prior
 557 can be used to restrict values to reasonable outcomes; e.g., for *G. ruber*, Mg/Ca values
 558 over 6.5 are rarely observed in the modern ocean (0% of core tops, 1% of sediment traps).
 559 To provide an example, as well as to test our model on out-of-sample data, we apply BAY-
 560 MAG to monthly average observations of SST, SSS, and pH at two locations that have

561 multi-year foraminiferal Mg/Ca sediment trap data (Fig. 7). For the Gulf of Mexico site,
 562 we used the SST, SSS, and pH climatologies (adjusted values) provided in the source pub-
 563 lication (Richey et al., 2019). For the Gulf of California site, we used average monthly
 564 SSTs reported in the source publication (McConnell & Thunell, 2005), WOA13 clima-
 565 tology for SSS, and pH climatology as estimated by Gray et al. (2018). Ω is set to 5.7
 566 for the Gulf of Mexico and 3.4 for the Gulf of California; since these values are high, they
 567 have minimal impact on predicted Mg/Ca. Both studies used a non-reductive cleaning
 568 protocol, so the cleaning value is set to 0. In all cases we use the group-specific, seasonal
 569 model; although temperatures and salinity vary month-by-month in this case, we assume
 570 that the seasonal model most accurately captures the ‘true’ environmental sensitivities.
 571 Weak priors on Mg/Ca were used to assign a low probability ($< 5\%$) to Mg/Ca values
 above 7 and 9 for *G. ruber* and *G. bulloides*, respectively (Fig. 7).

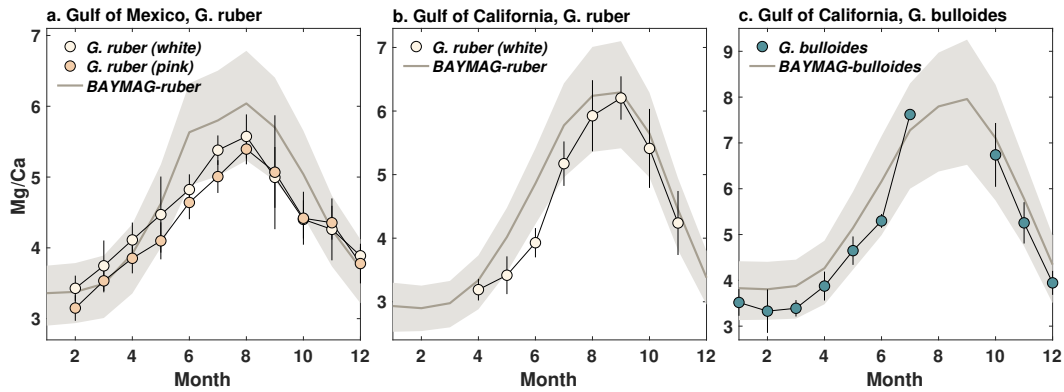


Figure 7. Forward-modeled Mg/Ca from BAYMAG, compared to sediment trap observations from the Gulf of Mexico (Richey et al., 2019) and Gulf of California (McConnell & Thunell, 2005). Normal priors of $\mathcal{N} \sim (4, 1.5)$ and $\mathcal{N} \sim (5, 2)$ were used for *G. ruber* and *G. bulloides*, respectively. The Gulf of Mexico data were shifted backwards by 1 month to account for sinking and integration time. No adjustments to the Gulf of California data were made; this is a shallower trap (485 m vs. 1150 m) and the data indicate minimal lag. Shading and error bars represent 1σ uncertainties.

572

573 Overall, the BAYMAG predictions match observed Mg/Ca values well, almost al-
 574 ways overlapping within the 1σ range (Fig. 7). This is an encouraging result, because
 575 our model is calibrated on core top foraminifera that have been affected by dissolution
 576 and sedimentary processes, while the sediment trap data consist of more pristine spec-
 577 imens. BAYMAG slightly overestimates *G. ruber* Mg/Ca in the Gulf of Mexico (Fig. 7a),
 578 even though our model residuals suggest that it should under-predict high values (Fig.
 579 6b), suggesting that the residual trends have a minimal impact on prediction.

580 6 Inversion of BAYMAG to predict past SST

581 Since BAYMAG is a multivariate model, inversion to predict past SSTs requires
 582 constraints on salinity, pH, and Ω . In the simplest case, these can be held constant at
 583 modern values, but this assumes that only temperature caused observed variation in Mg/Ca.
 584 More realistic inference can be derived from making informed assumptions about past
 585 changes in salinity, pH, and Ω . For example, over the Quaternary glacial cycles, it is re-
 586 asonable to assume that surface water pH and salinity both increased during glacial peri-
 587 ods due to lower atmospheric CO_2 and lower sea level. It is also possible to leverage
 588 information from independent proxies sensitive to changes in the oceanic carbonate sys-

tem, such as $\delta^{11}\text{B}$ (for surface pH) or benthic B/Ca (for Ω). Alternatively, output from a climate or biogeochemical model could be used to provide constraints on salinity, pH, and Ω .

To facilitate SST prediction for diverse applications, we provide two versions of the Bayesian inverse model for Mg/Ca. One assumes that salinity, pH, and Ω are known, allowing for quick computation of posterior SST. The other treats all of the environmental predictors as unknowns, and allows the user to place prior distributions on them. This latter model involves joint computation of posterior temperature, salinity, pH, and Ω and is therefore slower to converge, but has the advantage of propagating uncertainty in these co-variables into the estimation of SST.

To demonstrate use of the inverse models, we apply BAYMAG to three sites that have Late Quaternary Mg/Ca data as well as independent estimates of SST from alkenone $\text{U}_{37}^{K'}$ (Fig. 8a). In each case, we use the appropriate seasonal, group-specific model; however, for all three of these locations, our KDE method predicts a mean annual response. We draw modern Ω and surface pH value for each site from GLODAPv2 (Lauvset et al., 2016), and modern salinity from WOA13 (Boyer et al., 2013). In all cases, we use a prior standard deviation of 6°C , and assume that pH, salinity, and Ω are error-free; we found that including errors on these factors only slightly increases error bars, unless the errors are very large (not shown).

For the Holocene data at site MD99-2269 in the North Atlantic, we assume that salinity, and Ω are constant through time (*N. pachyderma* is not sensitive to pH). We find that BAYMAG predicts latest Holocene SST values that are in good agreement with modern observed annual SST, whereas the calibration (Elderfield & Ganssen, 2000) used in the original publication (Kristjánsdóttir et al., 2017) slightly underestimates SSTs (Fig. 8b). The BAYMAG predictions suggest that annual SSTs have declined through the Holocene by about 3°C . In contrast, the $\text{U}_{37}^{K'}$ data from this site show a weaker long-term trend, and are also much warmer than the *N. pachyderma* predictions (Fig. 8b). $\text{U}_{37}^{K'}$ at this latitude (66°N) is assumed to reflect late summer temperatures (August–October) (Tierney & Tingley, 2018); however modern August–October SSTs at this site (6.4°C) are still much cooler than the latest Holocene $\text{U}_{37}^{K'}$ values (ca. 9.5°C , Fig. 8b). This might indicate that $\text{U}_{37}^{K'}$ production is restricted to only the warmest of summer months; alternatively the warm bias could reflect the influence of sea ice. This site sits close to the boundary where substantial seasonal sea ice is present in the modern day, and anomalously high $\text{U}_{37}^{K'}$ values occur in areas of extensive sea ice cover (Filippova et al., 2016; Tierney & Tingley, 2018).

For site MD97-2120 in the South Pacific, we make some rudimentary assumptions of how pH and salinity may have varied over glacial-interglacial cycles, and use a prior standard deviation of 6°C . Following Gray et al. (2018) and Gray and Evans (2019), we assume that global pH increased by 0.13 units during the Last Glacial Maximum due to lowered CO_2 . We then scaled the normalized ice core CO_2 curve (Bereiter et al., 2015) to this value and added it to the modern site estimate of pH to simulate past changes. For this site, this results in a range of pH values between 8.12 (modern value) to 8.25 (maximum glacial value). For salinity, we scaled the normalized sea level curve to an inferred LGM change of 1.1 psu and added this to the site estimate, for a range between 34.4 (modern values) to 35.5 (maximum glacial value). We then interpolate these scaled curves to the ages at which there are Mg/Ca observations, and input them into BAYMAG. We do not explicitly account for the temperature effect on pH (e.g., Gray & Evans, 2019) because while it scales with the magnitude of local cooling, it is a small source of error for the LGM (0.65°C , Gray & Evans, 2019). Since the salinity and pH sensitivities are of opposite sign, the glacial-interglacial changes mostly cancel each other out, resulting in glacial SSTs that are only slightly warmer (ca. 0.5°C) than estimates made with constant salinity and pH (not shown).

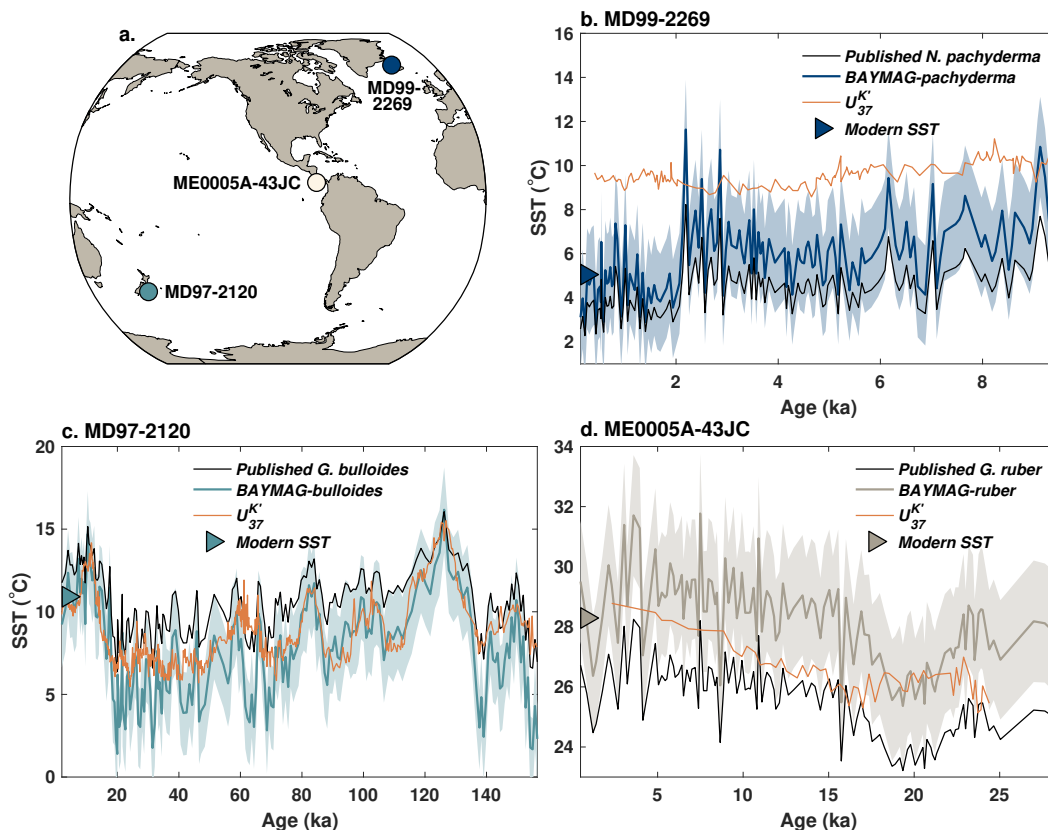


Figure 8. Example applications of BAYMAG to predict past SSTs. a) Locations of targeted Late Quaternary sites b) *N. pachyderma* data from MD99-2269 (66.6°N, 20.9°W, Kristjánssdóttir et al., 2017) c) *G. bulloides* data from MD97-2120 (45.5°S, 174.9°E, Pahnke et al., 2003) d) *G. ruber* data from ME0005A-43JC (7.9°N, 83.6°W, 1368 m, Benway et al., 2006). At each location, data are compared to $U_{37}^{K'}$ SST estimates (median values, calibrated with BAYSPLINE, Tierney & Tingley, 2018). Triangles show modern mean annual SSTs at each site. Shading indicates 1σ uncertainties.

641 The BAYMAG predictions from *G. bulloides* Mg/Ca at MD97-2120 produce lat-
 642 est Holocene SSTs in good agreement with modern mean annual values, and yield cooler
 643 median values and a larger glacial-interglacial range than the calibration (Mashiotta et
 644 al., 1999) used in the original publication (Pahnke et al., 2003) (Fig. 8c). There is gen-
 645 erally a good match with alkenone $U_{37}^{K'}$, except during the coldest times of the glacial
 646 periods (Fig. 8c). The cold predictions in part reflect the fact that the glacial *G. bul-*
 647 *loides* Mg/Ca values at this site are at the limit of the modern calibration dataset, and
 648 the group-specific model has a tendency to over-predict Mg/Ca (and thus under-predict
 649 SSTs) at southern latitudes (Fig. 6e). A tighter prior could mitigate this effect; how-
 650 ever, this example illustrates that caution should be exercised when extrapolating BAY-
 651 MAG to values of Mg/Ca that are near the edge or outside of the calibration range.

652 Finally, we tested BAYMAG on *G. ruber* data from site ME0005A-43JC, in the
 653 eastern Pacific warm pool. We scale salinity and pH estimates in the same manner as
 654 at site MD97-2120. Varying salinity and pH results in glacial estimates that are ca. 0.7°C
 655 warmer than a constant assumption (not shown). Latest Holocene BAYMAG predictions
 656 once again align well with modern SSTs, and are overall warmer than the published
 657 estimates (Benway et al., 2006), which used the Anand et al. (2003) calibration without

658 a correction for dissolution (Fig. 8d). Although this site is not particularly deep, it sits
 659 in a relatively corrosive location – modern Ω is 0.95 – thus BAYMAG assumes some Mg/Ca
 660 loss from dissolution. The magnitude of glacial cooling agrees well with the $U_{37}^{K'}$ estimates,
 661 although the two proxies have different trajectories through the deglaciation and the Holocene
 662 (Fig. 8d).

663 7 Use of BAYMAG on longer geological timescales

664 7.1 Incorporating changes in Mg/Ca of seawater

665 When Mg/Ca is used to infer SSTs on million-year timescales, data must be cor-
 666 rected for secular changes in the Mg/Ca ratio of seawater (Mg/Ca_{sw}). Ancient Mg/Ca_{sw}
 667 values can be independently estimated from fossil corals (Gothmann et al., 2015), halite
 668 fluid inclusions (Lowenstein et al., 2001; Horita et al., 2002; Brennan et al., 2013), cal-
 669 cium carbonate veins (Coggon et al., 2010), and echinoderm ossicles (Dickson, 2002, 2004).
 670 Although some of these Mg/Ca_{sw} estimates have large uncertainties, and are also some-
 671 times poorly dated, they clearly indicate a large, non-linear increase in Mg/Ca_{sw} over
 672 the past 200 Ma, with the most rapid change occurring in the last 30 Ma (Fig. 9a). The
 673 reason for the increase is still not certain; magnesium isotope evidence and geochemi-
 674 cal modeling suggests that it could reflect a decrease in Mg incorporation into marine
 675 clays as deep ocean waters cooled across the Cenozoic era (Higgins & Schrag, 2015).

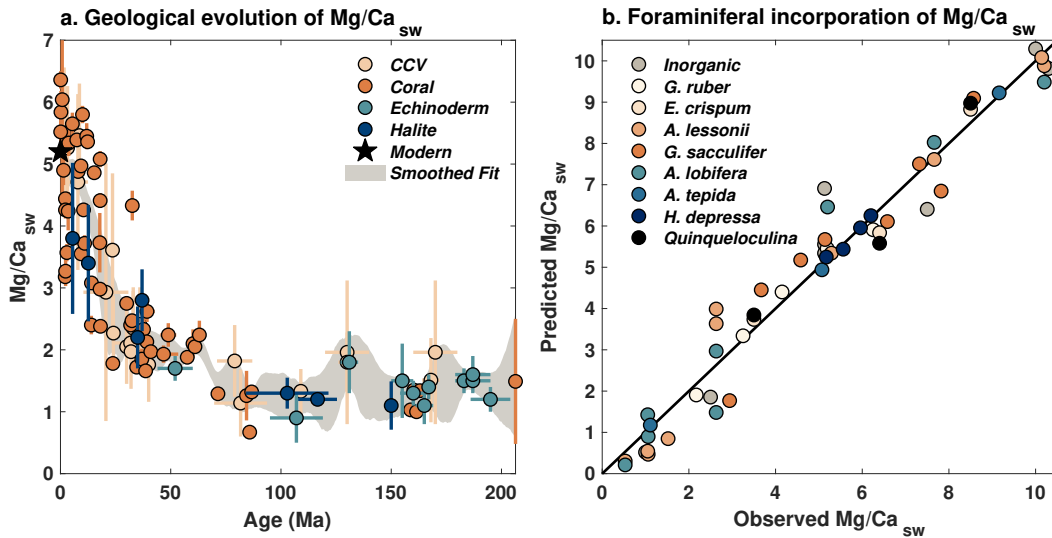


Figure 9. a. Evolution of Mg/Ca_{sw} over the past 200 Ma, according to Mg/Ca measured in calcium carbonate veins (Coggon et al., 2010), fossil corals (Gothmann et al., 2015), echinoderm ossicles (Dickson, 2002, 2004), and halite fluid inclusions (Lowenstein et al., 2001; Horita et al., 2002; Brennan et al., 2013). Star denotes the modern value of 5.2 mmol/mol (Horita et al., 2002). Shading encloses the 95% CI of an ensemble of Gaussian smoothed fits to the data, used in the seawater-enabled BAYMAG models. b. Relationship between observed Mg/Ca_{sw} and linear predictions of Mg/Ca_{sw} from Mg/Ca of calcite in laboratory inorganic precipitation (Mucci & Morse, 1983) and foraminiferal culture studies (Delaney et al., 1985; Segev & Erez, 2006; Raitzsch et al., 2010; Mewes et al., 2014; Evans, Brierley, et al., 2016; De Nooijer et al., 2017).

676 To develop a version of BAYMAG that accounts for changing Mg/Ca_{sw}, we cre-
 677 ated a 1,000-member ensemble of possible Mg/Ca_{sw} trajectories by Monte Carlo sam-
 678 pling the uncertainties in both age assignment and Mg/Ca_{sw} of each estimate in Fig-
 679 ure 9a, interpolating to a 0.5 Ma timestep, and applying a 13 Ma (the residence time of
 680 Mg) Gaussian smooth (Fig. 9a). The resulting collection of curves is then used to cal-
 681 culate Mg/Ca_{sw} for each time t for a given Mg/Ca data series, and then used in the pre-
 682 diction model, i.e.:

$$683 \ln(\text{Mg/Ca}) = \alpha_j + \mathbf{T} \cdot \beta_T + \mathbf{S} \cdot \beta_S + \mathbf{pH} \cdot \beta_P + \mathbf{\Omega}^{-2} \cdot \beta_O + (1 - \mathbf{clean} \cdot \beta_C) + \frac{\text{Mg/Ca}_{\text{sw}t}}{\text{Mg/Ca}_{\text{sw}0}} + \epsilon, \quad (8)$$

$$684 \epsilon \sim \mathcal{N}(\mathbf{0}, \sigma_i^2)$$

685 Previous work has suggested that the incorporation of Mg into calcite varies non-
 686 linearly with Mg/Ca_{sw}, necessitating a power function correction (Evans & Müller, 2012),
 687 rather than a simple ratio between the past value and the modern value as we suggest
 688 above. To re-examine whether such an adjustment is necessary, we compiled experimen-
 689 tal data in which planktic and benthic foraminifera were cultured at varying Mg/Ca_{sw}
 690 concentrations (Delaney et al., 1985; Segev & Erez, 2006; Raitzsch et al., 2010; Mewes
 691 et al., 2014; Evans, Brierley, et al., 2016; De Nooijer et al., 2017), along with an inor-
 692 ganic precipitation experiment (Mucci & Morse, 1983) (Fig. 9b). These data span val-
 693 ues of Mg/Ca_{sw} from 0.5 – 10 mmol/mol (Fig. 9b), which encompasses the range found
 694 throughout the Phanerozoic (0.5–6 mmol/mol, Dickson, 2002, 2004). For each species
 695 (and the inorganic experiment), we computed an ordinary least squares regression be-
 696 tween Mg/Ca_{sw} and Mg/Ca_c, and used the resulting coefficients to predict Mg/Ca_{sw} from
 697 Mg/Ca_c. If there were a non-linear relationship between Mg/Ca_{sw} and Mg/Ca_c, then
 698 the predictions should show curvature away from the the 1:1 line. We find that when all
 699 the experiments are considered together, this is not the case – a power function fit to the
 700 predictions, of the form $y = a \times x^b$, yields a value of b close to 1 (0.96 ± 0.08 , 2σ) sug-
 701 gesting no significant curvilinear behavior. Power fits to predictions from individual species
 702 (and the inorganic experiment) also yield values of b insignificantly different from 1, con-
 703 firming that the relationship between Mg/Ca_{sw} and Mg/Ca_c is adequately described by
 704 a linear function. The slope of this relationship varies substantially between species; how-
 705 ever, since Mg/Ca_{sw} is ratioed to the modern value (Eq. 8), this term cancels out. This
 706 analysis does not preclude non-linear incorporation of Mg into calcite at very low Mg/Ca_{sw}
 707 concentrations (<0.5 mmol/mol); however, such concentrations are not observed in the
 708 Phanerozoic. Thus, we conclude that a power function adjustment is not necessary for
 709 paleoclimate applications.

710 More recently, it has been proposed that the temperature sensitivity of Mg/Ca in
 711 foraminifera changes with Mg/Ca_{sw} (Evans, Brierley, et al., 2016). However, thus far this
 712 has only been detected in a culture experiment of *G. ruber*; a study of benthic foraminiferal
 713 species did not detect a change in temperature sensitivity with Mg/Ca_{sw} (De Nooijer
 714 et al., 2017). We therefore do not incorporate this aspect into our model; further exper-
 715 imental evidence supporting this effect is needed.

716 7.2 Applications

717 To test our Mg/Ca_{sw}-enabled models, we apply BAYMAG to representative Ceno-
 718 zoic Mg/Ca data. First, we use the seasonal, group-specific model to predict SSTs from
 719 *T. sacculifer* data from Site ODP 806, in the western Pacific warm pool (Wara et al.,
 720 2005). We assume that salinity and pH are constant through time and error-free, and
 721 use a prior standard deviation of 6°C (Fig. 10a). These data span the early Pliocene (5.3
 722 Ma) to present, over which time Mg/Ca_{sw} has evolved from 4.8 ± 0.2 (2σ) mmol/mol
 723 to the current value of 5.2 mmol/mol, according to our ensemble estimate. Although this

724 is a small change, it does impact SST prediction, as can be seen from comparison with
 725 the published SST estimates (Wara et al., 2005), which use the Dekens et al. (2002) cal-
 726 ibration and did not account for changing Mg/Ca_{sw} (Fig. 10a). Whereas the original
 727 SST estimates suggest that Pliocene SSTs were consistently cooler than modern, the BAY-
 728 MAG estimates indicate that they were mostly similar to, or warmer than, modern val-
 729 ues and bring the data into better agreement with independent estimates from the TEX_{86}
 730 proxy (Zhang et al., 2014) (Fig. 10a).

731 Next, we apply BAYMAG to Mg/Ca data from the Early Eocene Climatic Opti-
 732 mum (EECO, 53.3–49.1 Ma), one of the warmest times during the Cenozoic Era. These
 733 data include *Morozovella* spp. from site ODP 865 (Tripathi et al., 2003), hemipelagic out-
 734 crops from the eastern shore of New Zealand (mid-Waipara, Tawanui, Tora, and Hamp-
 735 den Beach, C. J. Hollis et al., 2009, 2012; Hines et al., 2017), and DSDP Site 277 (Hines
 736 et al., 2017). *Morozovella* spp. species are extinct, so we do not know their seasonal or
 737 depth habitat preferences. Thus, we use the pooled annual model, which provides generic
 738 constraints on temperature, salinity, pH, and Ω sensitivities. Following Evans et al. (2018),
 739 we assume, based on carbon modeling constraints (Tyrrell & Zeebe, 2004), that ocean
 740 pH is approximately 7.7 during the EECO. Since we have no good knowledge of how salin-
 741 ity changed, we hold it constant at a value of 34.5 for each site. For Ω , we test two as-
 742 sumptions: 1) that the foraminifera are essentially pristine, unaltered by seafloor disso-
 743 lution ($\Omega = 5$), and 2) that the foraminifera have experienced dissolution on par with
 744 what we would expect at the site locations today. For this latter assumption, we draw
 745 Ω from GLODAPv2 using the paleolatitude and paleolongitude (calculated from Baatsen
 746 et al. (2016), as suggested in C. Hollis et al. (2019)) and the inferred Eocene water depth
 747 as described in the original publication. We use an uninformative prior standard deviation
 748 of 10°C .

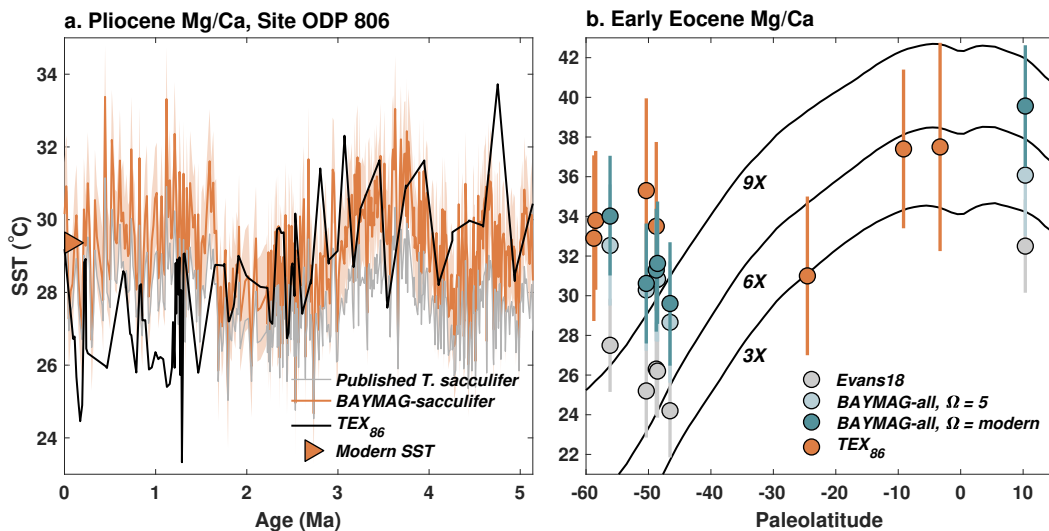


Figure 10. Application of BAYMAG to Cenozoic Mg/Ca data, with correction for changing Mg/Ca_{sw} . a) Mg/Ca data extending back to the Pliocene from Site ODP 806 (Wara et al., 2005). Triangle indicates modern mean annual SST. b) Mg/Ca data (Tripathi et al., 2003; C. J. Hollis et al., 2009, 2012; Hines et al., 2017) from the Early Eocene climatic optimum (53.3–49.1 Ma), plotted by paleolatitude. Black lines denote predicted SSTs from Eocene climate model simulations conducted under 3X, 6X, and 9X preindustrial CO_2 levels (Zhu et al., 2019). In both panels, TEX_{86} data (calibrated with BAYSPAR, Tierney & Tingley, 2014) are plotted for comparison. Shading and error bars represent 1σ uncertainties.

749 We compare our results to the inferences made by Evans et al. (2018) using the same
 750 Mg/Ca data, as well as independent estimates of SST from EECO TEX₈₆ data span-
 751 ning similar paleolatitudes (Pearson et al., 2007; Bijl et al., 2009; C. J. Hollis et al., 2009,
 752 2012; Bijl et al., 2013; Inglis et al., 2015; Cramwinckel et al., 2018) calibrated with BAYSPAR
 753 (Tierney & Tingley, 2014; C. Hollis et al., 2019) (Fig. 10b). All of the estimates from
 754 BAYMAG are warmer, on average, than those of Evans et al. (2018), by 4.5°C under the
 755 assumption of no dissolution, and by 5.8°C with modern Ω estimates (Fig. 10b). About
 756 1.6°C of this difference can be attributed to different assumptions about Mg/Ca_{sw} – our
 757 Gaussian smooth ensemble yields Mg/Ca_{sw} estimates for this time period of 2.0 ± 0.2
 758 mmol/mol (2σ), slightly lower than those of Evans et al. (2018) (2.2 ± 0.3 mmol/mol).
 759 The remainder of the difference reflects model form; Evans et al. (2018) first correct Mg/Ca
 760 for the pH effect using laboratory constraints (Evans, Wade, et al., 2016) and then cal-
 761 culate SST assuming a reduced temperature sensitivity at lower Mg/Ca_{sw}, using coef-
 762 ficients derived from *G. ruber* culture experiments (Evans, Brierley, et al., 2016).

763 In the absence of information concerning the Eocene carbonate system, Evans et
 764 al. (2018) assume no loss from dissolution at depth. For shallow and intermediate-depth
 765 sites considered here, allowing some dissolution increases median SST estimates up by
 766 0.3–1.5°C – a relatively minor effect. ODP 865 is an exception: here, using a modern
 767 estimate of Ω yields median SST estimates that are 3.5°C higher. This is because plate
 768 rotations (Herold et al., 2014; Baatsen et al., 2016) predict that this site was located much
 769 closer to the equator (4–10°N, vs. 18°N today) and farther east (138–144°W, vs. 179°W
 770 today) during the EECO. Today, the eastern equatorial Pacific is very corrosive, even
 771 at intermediate water depths. If EECO Pacific ocean chemistry was similar, then the Mg/Ca
 772 values at ODP 865 would imply very high SSTs (ca. 39°C, Fig. 10b). This illustrates
 773 how assumptions about Ω can have a large impact on SST estimation from Mg/Ca mea-
 774 sured in pelagic settings, especially over timescales when ocean chemistry may have changed
 775 substantially.

776 BAYMAG SST predictions agree more closely with EECO TEX₈₆ data than the
 777 Evans et al. (2018) calculations (Fig. 10b). Tropical SSTs inferred from Site 865 sup-
 778 port TEX₈₆ inferences of ca. 36°C, and match output from an Eocene climate model sim-
 779 ulation run under 6X preindustrial CO₂ (Zhu et al., 2019). The Mg/Ca predictions sup-
 780 port TEX₈₆ in detecting unusually high SSTs at sites near New Zealand (50–55°S pa-
 781 leolatitude) that are not easily explained by elevated CO₂; these data may reflect changes
 782 in ocean circulation leading to localized warming (C. J. Hollis et al., 2009) (Fig. 10b).

783 8 Conclusions

784 The Mg/Ca paleothermometer is complex. It is sensitive to multiple environmen-
 785 tal factors, which challenges both calibration and application. Traditionally, Mg/Ca ap-
 786 plications have “pre-corrected” the data for factors such as dissolution, laboratory clean-
 787 ing method, or pH sensitivity (e.g., Rosenthal & Lohmann, 2002; Evans et al., 2018; Gray
 788 & Evans, 2019). While effective, this makes uncertainty propagation challenging. A clear
 789 advantage of our BAYMAG models is that all known environmental sensitivities are in-
 790 cluded in a single model framework, making pre-correction obsolete. Furthermore, we
 791 show that we can account for most of the variance in the Mg/Ca of core top data through
 792 use of a hierarchical Bayesian model structure that leverages both culture and core top
 793 constraints on environmental sensitivities. Encouragingly, temperature remains the most
 794 important predictor of Mg/Ca, followed by bottom water calcite saturation state (Ω).
 795 Salinity and pH sensitivities are essentially undetectable in core top data; hence culture
 796 constraints are key.

797 The BAYMAG hierarchical models fit the data well, although some species, most
 798 notably *G. ruber*, still have trends in their residuals suggesting that some variance is left
 799 unexplained. Future work will be needed to identify why this is the case; we hypothe-

800 size that there is latent co-variate that scales with temperature (possibly pH). Fortunately,
 801 the absolute magnitude of the residuals is small, such that the trends typically don't bias
 802 predicted values. Indeed, applications of BAYMAG demonstrate that it yields reason-
 803 able forward predictions of Mg/Ca when compared to sediment trap observations, and
 804 reasonable inverse predictions when compared to independent SST proxies. The latter
 805 is true even though strong – and potentially incorrect – assumptions about past changes
 806 in Ω , salinity, and pH must be made. Deep time applications must additionally account
 807 for changing Mg/Ca_{sw}. We use independent constraints on the evolution of Mg/Ca_{sw}
 808 to develop a smoothed ensemble estimate for use with BAYMAG. Example applications
 809 once again suggest good agreement with independent SST proxies, but there can be large
 810 uncertainties in absolute SST estimates when potential changes in Ω in particular are
 811 considered.

812 In this work, we seek to develop prediction models for Mg/Ca of foraminifera that
 813 are independent from other proxy systems. However, given the multivariate nature of
 814 Mg/Ca, it would be beneficial to leverage information from independent temperature prox-
 815 ies in a formal hierarchical model structure. Previous work has already explored this av-
 816 enue by combining Mg/Ca measurements with TEX₈₆ or $\Delta 47$ to estimate Mg/Ca_{sw} (e.g.,
 817 O'Brien et al., 2014; Evans, Brierley, et al., 2016; Evans et al., 2018) and by combining
 818 Mg/Ca with $\delta^{18}\text{O}$ to infer $\delta^{18}\text{O}_{sw}$ or salinity (e.g., Oppo et al., 2009; Thirumalai et al.,
 819 2016; Tierney et al., 2016). Future work might explore incorporating $\delta^{11}\text{B}$ and B/Ca es-
 820 timates of pH and calcite saturation state, respectively. This would almost certainly im-
 821 prove past estimates of SST, especially over timescales when ocean carbonate chemistry
 822 is expected to have changed substantially.

823 Appendix A Bayesian regression model priors

824 Priors for the Bayesian regression parameters were chosen so as to enforce the ex-
 825 pected direction of the sensitivity based on geochemistry (e.g., Mg/Ca increases with tem-
 826 perature but decreases with Ω^{-2}) but otherwise be only weakly informative, with the
 827 exception of the salinity prior. The salinity sensitivity was explicitly bounded by the pos-
 828 terior value for β_S from culture data ($4.3 \pm 1.3\%$, 2σ) to counteract the tendency of the
 829 core tops to dilute the sensitivity. Slightly different priors for the pooled and group-specific
 830 models were used for the $\sigma_{\beta T_c}$ and σ parameters:

$$\begin{aligned}
 831 \quad & \alpha \sim \mathcal{U}(-5, 10), \\
 832 \quad & \mu_{\beta T_c} \sim \mathcal{N}_{[0, \infty)}(0.07, 0.015), \\
 833 \quad & \sigma_{\beta T_c} \sim \text{HalfCauchy}(0.02)_{[\text{pooled}]}; \sim \text{HalfCauchy}(0.015)_{[\text{species}]} \\
 834 \quad & \beta_S \sim \mathcal{N}_{[0, \infty)}(0.043, 0.0065), \\
 835 \quad & \beta_P \sim \mathcal{N}_{(\infty, 0]}(-0.7, 0.2), \\
 836 \quad & \beta_O \sim \mathcal{N}_{(\infty, 0]}(-0.2, 0.2), \\
 837 \quad & \beta_C \sim \mathcal{N}_{[0, \infty)}(0.12, 0.1), \\
 838 \quad & \sigma \sim \mathcal{U}(0, 0.5)_{[\text{pooled}]}; \sim \mathcal{U}(0, 0.3)_{[\text{species}]} \tag{A1}
 \end{aligned}$$

839 Plots of the prior vs. posterior distributions for the pooled annual and group-specific sea-
 840 sonal models are shown below. Note that the temperature panel contains posteriors for
 841 the hyperparameter $\mu_{\beta T_c}$, the culture data parameter β_{T_c} , and the core top data param-
 842 eter β_T .

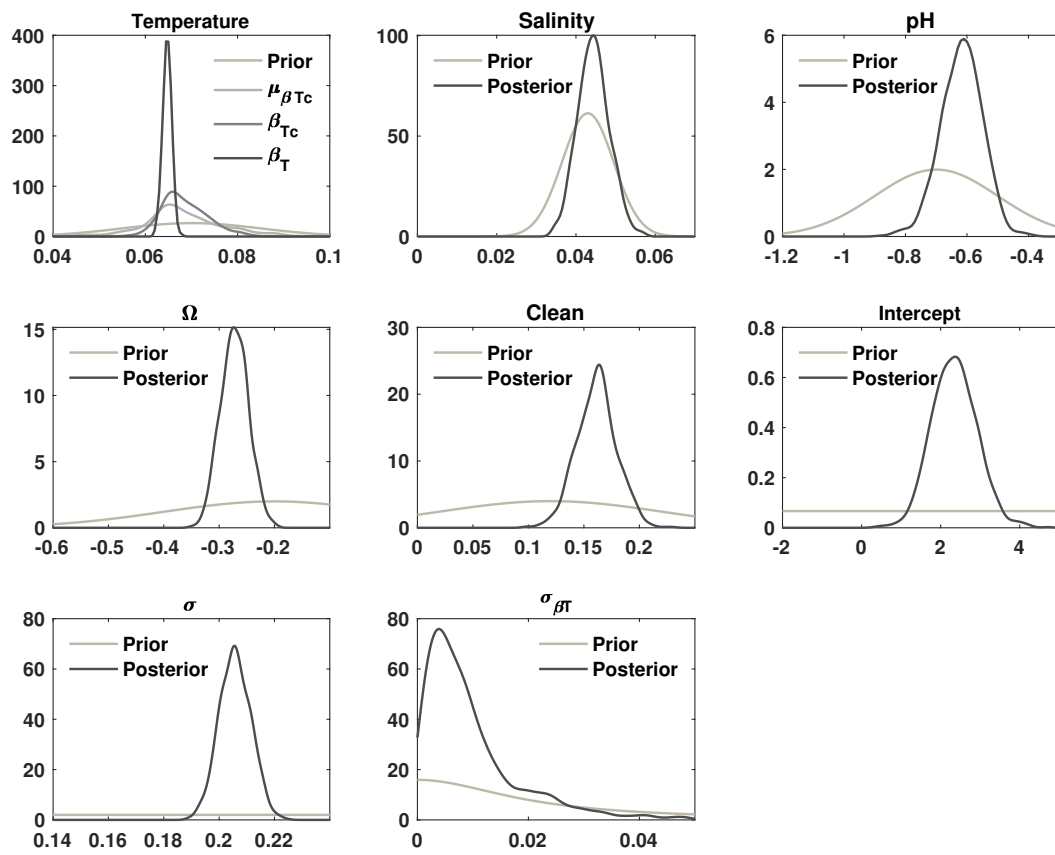


Figure A1. Prior and posterior parameter distributions for the pooled annual model.

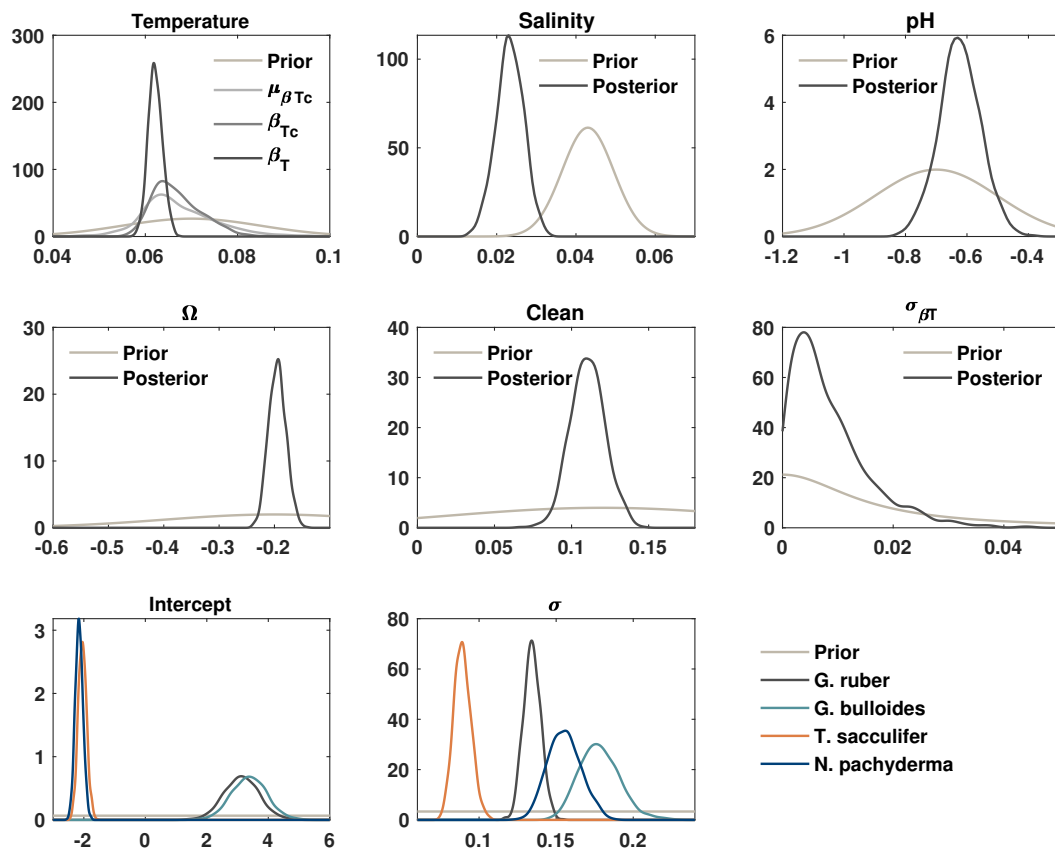


Figure A2. Prior and posterior parameter distributions for the group-specific seasonal model.

Acknowledgments

This work was supported by National Science Foundation grant AGS #1602301, the Heising-Simons Foundation, and the Packard Fellowship in Science and Engineering to JT. BAYMAG code (in MATLAB) is available on GitHub: <https://github.com/jesstierney/BAYMAG>. Compiled core top and culture data are available as Supplementary Data, as well as on-line in the NOAA NCEI Paleoclimatology archive: [insert link here when ready].

References

- Aagaard-Sørensen, S., Husum, K., Hald, M., Marchitto, T., & Godtlielsen, F. (2014). Sub sea surface temperatures in the Polar North Atlantic during the Holocene: Planktic foraminiferal Mg/Ca temperature reconstructions. *The Holocene*, *24*(1), 93–103.
- Allen, K. A., Hönisch, B., Eggins, S. M., Haynes, L. L., Rosenthal, Y., & Yu, J. (2016). Trace element proxies for surface ocean conditions: A synthesis of culture calibrations with planktic foraminifera. *Geochimica et Cosmochimica Acta*, *193*, 197–221.
- Anand, P., Elderfield, H., & Conte, M. H. (2003). Calibration of Mg/Ca thermometry in planktonic foraminifera from a sediment trap time series. *Paleoceanography*, *18*(2).
- Arbuszewski, J., deMenocal, P., Kaplan, A., & Farmer, E. C. (2010). On the fidelity of shell-derived $\delta^{18}\text{O}$ seawater estimates. *Earth and Planetary Science Letters*, *300*(3), 185–196.
- Arbuszewski, J. A., Cléroux, C., Bradtmiller, L., & Mix, A. (2013). Meridional shifts of the Atlantic intertropical convergence zone since the Last Glacial Maximum. *Nature Geoscience*, *6*(11), 959–962.
- Aurahs, R., Treis, Y., Darling, K., & Kucera, M. (2011). A revised taxonomic and phylogenetic concept for the planktonic foraminifer species *Globigerinoides ruber* based on molecular and morphometric evidence. *Marine Micropaleontology*, *79*(1-2), 1–14.
- Baatsen, M., Van Hinsbergen, D. J., Heydt, A. S., Dijkstra, H. A., Sluijs, A., Abels, H. A., & Bijl, P. K. (2016). Reconstructing geographical boundary conditions for palaeoclimate modelling during the Cenozoic. *Climate of the Past*, *12*(8), 1635–1644.
- Barker, S., Cacho, I., Benway, H., & Tachikawa, K. (2005). Planktonic foraminiferal Mg/Ca as a proxy for past oceanic temperatures: a methodological overview and data compilation for the Last Glacial Maximum. *Quaternary Science Reviews*, *24*(7), 821–834.
- Barker, S., Greaves, M., & Elderfield, H. (2003). A study of cleaning procedures used for foraminiferal Mg/Ca paleothermometry. *Geochemistry, Geophysics, Geosystems*, *4*(9).
- Benway, H. M., Mix, A. C., Haley, B. A., & Klinkhammer, G. P. (2006). Eastern Pacific Warm Pool paleosalinity and climate variability: 0–30 kyr. *Paleoceanography*, *21*(3).
- Bereiter, B., Eggleston, S., Schmitt, J., Nehrbass-Ahles, C., Stocker, T. F., Fischer, H., . . . Chappellaz, J. (2015). Revision of the EPICA Dome C CO₂ record from 800 to 600 kyr before present. *Geophysical Research Letters*, *42*(2), 542–549.
- Berger, W. H. (1970). Planktonic foraminifera: selective solution and the lysocline. *Marine Geology*, *8*(2), 111–138.
- Bijl, P. K., Bendle, J. A., Bohaty, S. M., Pross, J., Schouten, S., Tauxe, L., . . . Expedition 318 Scientists (2013). Eocene cooling linked to early flow across the Tasmanian Gateway. *Proceedings of the National Academy of Sciences*, *110*(24), 9645–9650.
- Bijl, P. K., Schouten, S., Sluijs, A., Reichert, G.-J., Zachos, J. C., & Brinkhuis, H.

- 896 (2009). Early palaeogene temperature evolution of the southwest Pacific ocean.
897 *Nature*, 461(7265), 776–779.
- 898 Boussetta, S., Kallel, N., Bassinot, F., Labeyrie, L., Duplessy, J.-C., Caillon, N., ...
899 Rebaubier, H. (2012). Mg/Ca-paleothermometry in the western Mediterranean
900 Sea on planktonic foraminifer species *Globigerina bulloides*: Constraints and
901 implications. *Comptes Rendus Geoscience*, 344(5), 267–276.
- 902 Boyer, T. P., Antonov, J. I., Baranova, O. K., Coleman, C., Garcia, H. E., Grodsky,
903 A., ... Zweng, M. (2013). *World ocean database 2013* (Tech. Rep.). Silver
904 Spring, MD: NOAA.
- 905 Boyle, E., & Keigwin, L. (1985). Comparison of Atlantic and Pacific paleochemi-
906 cal records for the last 215,000 years: Changes in deep ocean circulation and
907 chemical inventories. *Earth and Planetary Science Letters*, 76(1), 135–150.
- 908 Brennan, S. T., Lowenstein, T. K., & Cendón, D. I. (2013). The major-ion compo-
909 sition of Cenozoic seawater: The past 36 million years from fluid inclusions in
910 marine halite. *American Journal of Science*, 313(8), 713–775.
- 911 Brown, S. J., & Elderfield, H. (1996). Variations in Mg/Ca and Sr/Ca ratios of
912 planktonic foraminifera caused by postdepositional dissolution: Evidence of
913 shallow Mg-dependent dissolution. *Paleoceanography*, 11(5), 543–551.
- 914 Carpenter, B., Gelman, A., Hoffman, M. D., Lee, D., Goodrich, B., Betancourt, M.,
915 ... Riddell, A. (2017). Stan: A probabilistic programming language. *Journal*
916 *of Statistical Software*, 76(1).
- 917 Cléroux, C., Cortijo, E., Anand, P., Labeyrie, L., Bassinot, F., Caillon, N., & Du-
918 plessy, J.-C. (2008). Mg/Ca and Sr/Ca ratios in planktonic foraminifera:
919 Proxies for upper water column temperature reconstruction. *Paleoceanography*
920 *and Paleoclimatology*, 23(3).
- 921 Coggon, R. M., Teagle, D. A., Smith-Duque, C. E., Alt, J. C., & Cooper, M. J.
922 (2010). Reconstructing past seawater Mg/Ca and Sr/Ca from mid-ocean ridge
923 flank calcium carbonate veins. *Science*, 327(5969), 1114–1117.
- 924 Cramwinckel, M. J., Huber, M., Kocken, I. J., Agnini, C., Bijl, P. K., Bohaty, S. M.,
925 ... Sluijs, A. (2018). Synchronous tropical and polar temperature evolution in
926 the Eocene. *Nature*, 559(7714), 382–386.
- 927 Dahl, K. A., & Oppo, D. W. (2006). Sea surface temperature pattern reconstruc-
928 tions in the Arabian Sea. *Paleoceanography*, 21(1).
- 929 Darling, K. F., Kucera, M., Kroon, D., & Wade, C. M. (2006). A resolution for the
930 coiling direction paradox in *Neogloboquadrina pachyderma*. *Paleoceanography*,
931 21(2).
- 932 Davis, C. V., Fehrenbacher, J. S., Hill, T. M., Russell, A. D., & Spero, H. J. (2017).
933 Relationships Between Temperature, pH, and Crusting on Mg/Ca Ratios in
934 Laboratory-Grown *Neogloboquadrina* Foraminifera. *Paleoceanography*, 32(11),
935 1137–1152.
- 936 de Garidel-Thoron, T., Rosenthal, Y., Beaufort, L., Bard, E., Sonzogni, C., & Mix,
937 A. C. (2007). A multiproxy assessment of the western equatorial Pacific
938 hydrography during the last 30 kyr. *Paleoceanography*, 22(3).
- 939 Dekens, P. S., Lea, D. W., Pak, D. K., & Spero, H. J. (2002). Core top calibration
940 of Mg/Ca in tropical foraminifera: Refining paleotemperature estimation. *Geo-*
941 *chemistry, Geophysics, Geosystems*, 3(4), 1–29.
- 942 Delaney, M. L., Bé, A. W., & Boyle, E. A. (1985). Li, Sr, Mg, and Na in
943 foraminiferal calcite shells from laboratory culture, sediment traps, and sed-
944 iment cores. *Geochimica et Cosmochimica Acta*, 49(6), 1327–1341.
- 945 De Nooijer, L., Van Dijk, I., Toyofuku, T., & Reichert, G. (2017). The impacts
946 of seawater Mg/Ca and temperature on element incorporation in benthic
947 foraminiferal calcite. *Geochemistry, Geophysics, Geosystems*, 18(10), 3617–
948 3630.
- 949 Dickson, J. (2002). Fossil echinoderms as monitor of the Mg/Ca ratio of Phanerozoic
950 oceans. *Science*, 298(5596), 1222–1224.

- 951 Dickson, J. (2004). Echinoderm skeletal preservation: calcite-aragonite seas and the
 952 Mg/Ca ratio of Phanerozoic oceans. *Journal of Sedimentary Research*, 74(3),
 953 355–365.
- 954 Dueñas-Bohórquez, A., da Rocha, R. E., Kuroyanagi, A., Bijma, J., & Reichart, G.-
 955 J. (2009). Effect of salinity and seawater calcite saturation state on Mg and Sr
 956 incorporation in cultured planktonic foraminifera. *Marine Micropaleontology*,
 957 73(3), 178–189.
- 958 Dyez, K. A., Zahn, R., & Hall, I. R. (2014). Multicentennial Agulhas leakage vari-
 959 ability and links to North Atlantic climate during the past 80,000 years. *Paleo-*
 960 *ceanography*, 29(12), 1238–1248.
- 961 Elderfield, H., & Ganssen, G. (2000). Past temperature and $\delta^{18}\text{O}$ of surface ocean
 962 waters inferred from foraminiferal Mg/Ca ratios. *Nature*, 405(6785), 442–445.
- 963 Elderfield, H., Vautravers, M., & Cooper, M. (2002). The relationship between shell
 964 size and Mg/Ca, Sr/Ca, $\delta^{18}\text{O}$, and $\delta^{13}\text{C}$ of species of planktonic foraminifera.
 965 *Geochemistry, Geophysics, Geosystems*, 3(8), 1–13.
- 966 Erez, J., & Honjo, S. (1981). Comparison of isotopic composition of planktonic
 967 foraminifera in plankton tows, sediment traps and sediments. *Palaeogeography*,
 968 *Palaeoclimatology, Palaeoecology*, 33(1-3), 129–156.
- 969 Evans, D., Brierley, C., Raymo, M. E., Erez, J., & Müller, W. (2016). Plank-
 970 tic foraminifera shell chemistry response to seawater chemistry: Pliocene–
 971 Pleistocene seawater Mg/Ca, temperature and sea level change. *Earth and*
 972 *Planetary Science Letters*, 438, 139–148.
- 973 Evans, D., & Müller, W. (2012). Deep time foraminifera Mg/Ca paleothermometry:
 974 Nonlinear correction for secular change in seawater Mg/Ca. *Paleoceanography*
 975 *and Paleoclimatology*, 27(4).
- 976 Evans, D., Sagoo, N., Renema, W., Cotton, L. J., Müller, W., Todd, J. A., ... Af-
 977 fek, H. P. (2018). Eocene greenhouse climate revealed by coupled clumped
 978 isotope-Mg/Ca thermometry. *Proceedings of the National Academy of Sci-*
 979 *ences*, 201714744.
- 980 Evans, D., Wade, B. S., Henehan, M., Erez, J., & Müller, W. (2016). Revisiting
 981 carbonate chemistry controls on planktic foraminifera Mg/Ca: implications for
 982 sea surface temperature and hydrology shifts over the Paleocene–Eocene Ther-
 983 mal Maximum and Eocene–Oligocene transition. *Climate of the Past*, 12(4),
 984 819–835.
- 985 Fairbanks, R. G., Wiebe, P. H., & Bé, A. W. (1980). Vertical distribution and
 986 isotopic composition of living planktonic foraminifera in the western North
 987 Atlantic. *Science*, 207(4426), 61–63.
- 988 Fallet, U., Castañeda, I. S., Henry-Edwards, A., Richter, T. O., Boer, W., Schouten,
 989 S., & Brummer, G.-J. (2012). Sedimentation and burial of organic and in-
 990 organic temperature proxies in the Mozambique Channel, SW Indian Ocean.
 991 *Deep Sea Research Part I: Oceanographic Research Papers*, 59, 37–53.
- 992 Farmer, E. C., Demenocal, P. B., & Marchitto, T. M. (2005). Holocene and deglacial
 993 ocean temperature variability in the Benguela upwelling region: Implications
 994 for low-latitude atmospheric circulation. *Paleoceanography*, 20(2).
- 995 Ferguson, J., Henderson, G., Kucera, M., & Rickaby, R. (2008). Systematic change
 996 of foraminiferal Mg/Ca ratios across a strong salinity gradient. *Earth and*
 997 *Planetary Science Letters*, 265(1), 153–166.
- 998 Filippova, A., Kienast, M., Frank, M., & Schneider, R. (2016). Alkenone paleother-
 999 mometry in the North Atlantic: A review and synthesis of surface sediment
 1000 data and calibrations. *Geochemistry, Geophysics, Geosystems*, 17(4), 1370–
 1001 1382.
- 1002 Friedrich, O., Schiebel, R., Wilson, P. A., Weldeab, S., Beer, C. J., Cooper, M. J., &
 1003 Fiebig, J. (2012). Influence of test size, water depth, and ecology on Mg/Ca,
 1004 Sr/Ca, $\delta^{18}\text{O}$ and $\delta^{13}\text{C}$ in nine modern species of planktic foraminifers. *Earth*
 1005 *and Planetary Science Letters*, 319, 133–145.

- 1006 Ganssen, G., & Kroon, D. (2000). The isotopic signature of planktonic foraminifera
1007 from NE Atlantic surface sediments: implications for the reconstruction of past
1008 oceanic conditions. *Journal of the Geological Society*, *157*(3), 693–699.
- 1009 Gebregiorgis, D., Hathorne, E. C., Sijinkumar, A., Nath, B. N., Nürnberg, D., &
1010 Frank, M. (2016). South Asian summer monsoon variability during the last
1011 ~54 kyrs inferred from surface water salinity and river runoff proxies. *Quater-
1012 nary Science Reviews*, *138*, 6–15.
- 1013 Gelman, A., Carlin, J., Stern, H., & Rubin, D. (2003). *Bayesian data analysis* (2nd
1014 ed.). Boca Raton: Chapman & Hall/CRC.
- 1015 Gibbons, F. T., Oppo, D. W., Mohtadi, M., Rosenthal, Y., Cheng, J., Liu, Z., &
1016 Linsley, B. K. (2014). Deglacial $\delta^{18}\text{O}$ and hydrologic variability in the trop-
1017 ical Pacific and Indian Oceans. *Earth and Planetary Science Letters*, *387*,
1018 240–251.
- 1019 Gothmann, A. M., Stolarski, J., Adkins, J. F., Schoene, B., Dennis, K. J., Schrag,
1020 D. P., ... Bender, M. L. (2015). Fossil corals as an archive of secular varia-
1021 tions in seawater chemistry since the Mesozoic. *Geochimica et Cosmochimica
1022 Acta*, *160*, 188–208.
- 1023 Gray, W. R., & Evans, D. (2019). Non-thermal influences on Mg/Ca in plank-
1024 tonic foraminifera: A review of culture studies and application to the Last
1025 Glacial Maximum. *Paleoceanography and Paleoclimatology*, *34*. doi:
1026 <https://doi.org/10.1029/2018PA003517>
- 1027 Gray, W. R., Weldeab, S., Lea, D. W., Rosenthal, Y., Gruber, N., Donner, B., &
1028 Fischer, G. (2018). The effects of temperature, salinity, and the carbonate
1029 system on Mg/Ca in *Globigerinoides ruber* (white): A global sediment trap
1030 calibration. *Earth and Planetary Science Letters*, *482*, 607–620.
- 1031 Hastings, D. W., Russell, A. D., & Emerson, S. R. (1998). Foraminiferal magne-
1032 sium in *Globigerinoides sacculifer* as a paleotemperature proxy. *Paleoceanogra-
1033 phy and Paleoclimatology*, *13*(2), 161–169.
- 1034 Herold, N., Buzan, J., Seton, M., Goldner, A., Green, J., Müller, R., ... Huber, M.
1035 (2014). A suite of early Eocene (~55 Ma) climate model boundary conditions.
1036 *Geoscientific Model Development*, *7*(5), 2077–2090.
- 1037 Hertzberg, J. E., & Schmidt, M. W. (2013). Refining *Globigerinoides ruber* Mg/Ca
1038 paleothermometry in the Atlantic Ocean. *Earth and Planetary Science Letters*,
1039 *383*, 123–133.
- 1040 Higgins, J. A., & Schrag, D. P. (2015). The Mg isotopic composition of Cenozoic
1041 seawater—evidence for a link between Mg-clays, seawater Mg/Ca, and climate.
1042 *Earth and Planetary Science Letters*, *416*, 73–81.
- 1043 Hines, B. R., Hollis, C. J., Atkins, C. B., Baker, J. A., Morgans, H. E., & Strong,
1044 P. C. (2017). Reduction of oceanic temperature gradients in the early eocene
1045 southwest pacific ocean. *Palaeogeography, palaeoclimatology, palaeoecology*,
1046 *475*, 41–54.
- 1047 Hollis, C., Dunkley Jones, T., Anagnostou, E., Bijl, P., Cramwinckel, M., Cui, Y.,
1048 ... Lunt, D. (2019). The DeepMIP contribution to PMIP4: methodologies
1049 for selection, compilation and analysis of latest Paleocene and early Eocene
1050 climate proxy data, incorporating version 0.1 of the DeepMIP database. *Geo-
1051 scientific Model Development Discussions*.
- 1052 Hollis, C. J., Handley, L., Crouch, E. M., Morgans, H. E., Baker, J. A., Creech, J.,
1053 ... Pancost, R. (2009). Tropical sea temperatures in the high-latitude South
1054 Pacific during the Eocene. *Geology*, *37*(2), 99–102.
- 1055 Hollis, C. J., Taylor, K. W., Handley, L., Pancost, R. D., Huber, M., Creech, J. B.,
1056 ... Zachos, J. C. (2012). Early Paleogene temperature history of the South-
1057 west Pacific Ocean: Reconciling proxies and models. *Earth and Planetary
1058 Science Letters*, *349*, 53–66.
- 1059 Hollstein, M., Mohtadi, M., Rosenthal, Y., Moffa Sanchez, P., Oppo, D.,
1060 Martínez Méndez, G., ... Hebbeln, D. (2017). Stable oxygen isotopes and

- 1061 Mg/Ca in Planktic foraminifera from modern surface sediments of the Western
 1062 Pacific Warm Pool: Implications for thermocline reconstructions. *Paleoceanog-*
 1063 *raphy*, *32*(11), 1174–1194.
- 1064 Hönisch, B., Allen, K. A., Lea, D. W., Spero, H. J., Eggins, S. M., Arbuszewski,
 1065 J., ... Elderfield, H. (2013). The influence of salinity on Mg/Ca in planktic
 1066 foraminifers—Evidence from cultures, core-top sediments and complementary
 1067 $\delta^{18}\text{O}$. *Geochimica et Cosmochimica Acta*, *121*, 196–213.
- 1068 Horita, J., Zimmermann, H., & Holland, H. D. (2002). Chemical evolution of seawater
 1069 during the Phanerozoic: Implications from the record of marine evaporites.
 1070 *Geochimica et Cosmochimica Acta*, *66*(21), 3733–3756.
- 1071 Inglis, G. N., Farnsworth, A., Lunt, D., Foster, G. L., Hollis, C. J., Pagani, M., ...
 1072 Pancost, R. (2015). Descent toward the Icehouse: Eocene sea surface cooling
 1073 inferred from GDGT distributions. *Paleoceanography*, *30*(7), 1000–1020.
- 1074 Johnstone, H. J., Yu, J., Elderfield, H., & Schulz, M. (2011). Improving temperature
 1075 estimates derived from Mg/Ca of planktonic foraminifera using X-ray com-
 1076 puted tomography-based dissolution index, XDX. *Paleoceanography*, *26*(1).
- 1077 Keigwin, L. D., Sachs, J. P., Rosenthal, Y., & Boyle, E. A. (2005). The 8200 year
 1078 BP event in the slope water system, western subpolar North Atlantic. *Paleo-*
 1079 *ceanography*, *20*(2).
- 1080 Khider, D., Huerta, G., Jackson, C., Stott, L., & Emile-Geay, J. (2015). A Bayesian,
 1081 multivariate calibration for *Globigerinoides ruber* Mg/Ca. *Geochemistry, Geo-*
 1082 *physics, Geosystems*, *16*(9), 2916–2932.
- 1083 Kisakürek, B., Eisenhauer, A., Böhm, F., Garbe-Schönberg, D., & Erez, J. (2008).
 1084 Controls on shell Mg/Ca and Sr/Ca in cultured planktonic foraminiferan,
 1085 *Globigerinoides ruber* (white). *Earth and Planetary Science Letters*, *273*,
 1086 260–269.
- 1087 Kozdon, R., Eisenhauer, A., Weinelt, M., Meland, M. Y., & Nürnberg, D. (2009).
 1088 Reassessing Mg/Ca temperature calibrations of *Neogloboquadrina pachyderma*
 1089 (sinistral) using paired $\delta^{44/40}\text{Ca}$ and Mg/Ca measurements. *Geochemistry,*
 1090 *Geophysics, Geosystems*, *10*(3).
- 1091 Kristjánsdóttir, G. B., Moros, M., Andrews, J. T., & Jennings, A. E. (2017).
 1092 Holocene Mg/Ca, alkenones, and light stable isotope measurements on the
 1093 outer North Iceland shelf (MD99-2269): A comparison with other multi-proxy
 1094 data and sub-division of the Holocene. *The Holocene*, *27*(1), 52–62.
- 1095 Kubota, Y., Kimoto, K., Tada, R., Oda, H., Yokoyama, Y., & Matsuzaki, H. (2010).
 1096 Variations of East Asian summer monsoon since the last deglaciation based on
 1097 Mg/Ca and oxygen isotope of planktic foraminifera in the northern East China
 1098 Sea. *Paleoceanography and Paleoclimatology*, *25*(4).
- 1099 Lauvset, S. K., Key, R. M., Olsen, A., van Heuven, S., Velo, A., Lin, X., ... Wa-
 1100 telet, S. (2016). A new global interior ocean mapped climatology: the 1×1
 1101 GLODAP version 2. *Earth System Science Data*, *8*, 325–340.
- 1102 Lea, D. W., Mashiotta, T. A., & Spero, H. J. (1999). Controls on magnesium and
 1103 strontium uptake in planktonic foraminifera determined by live culturing.
 1104 *Geochimica et Cosmochimica Acta*, *63*(16), 2369–2379.
- 1105 Lea, D. W., Pak, D. K., Belanger, C. L., Spero, H. J., Hall, M. A., & Shackleton,
 1106 N. J. (2006). Paleoclimate history of Galapagos surface waters over the last
 1107 135,000 yr. *Quaternary Science Reviews*, *25*(11-12), 1152–1167.
- 1108 Lea, D. W., Pak, D. K., Peterson, L. C., & Hughen, K. A. (2003). Synchronicity of
 1109 tropical and high-latitude Atlantic temperatures over the last glacial termina-
 1110 tion. *science*, *301*(5638), 1361–1364.
- 1111 Lea, D. W., Pak, D. K., & Spero, H. J. (2000). Climate impact of late Quater-
 1112 nary equatorial Pacific sea surface temperature variations. *Science*, *289*(5485),
 1113 1719–1724.
- 1114 Leduc, G., Vidal, L., Tachikawa, K., Rostek, F., Sonzogni, C., Beaufort, L., & Bard,
 1115 E. (2007). Moisture transport across Central America as a positive feedback

- 1116 on abrupt climatic changes. *Nature*, 445(7130), 908–911.
- 1117 Levi, C., Labeyrie, L., Bassinot, F., Guichard, F., Cortijo, E., Waelbroeck, C., ...
 1118 Elderfield, H. (2007). Low-latitude hydrological cycle and rapid climate
 1119 changes during the last deglaciation. *Geochemistry, Geophysics, Geosystems*,
 1120 8(5).
- 1121 Linsley, B. K., Rosenthal, Y., & Oppo, D. W. (2010). Holocene evolution of the In-
 1122 donesian throughflow and the western Pacific warm pool. *Nature Geoscience*,
 1123 3(8), 578.
- 1124 Lombard, F., Labeyrie, L., Michel, E., Bopp, L., Cortijo, E., Retailleau, S., ... Joris-
 1125 sen, F. (2011). Modelling planktic foraminifer growth and distribution using
 1126 an ecophysiological multi-species approach. *Biogeosciences*, 8(4), 853–873.
- 1127 Lombard, F., Labeyrie, L., Michel, E., Spero, H. J., & Lea, D. W. (2009). Modelling
 1128 the temperature dependent growth rates of planktic foraminifera. *Marine Mi-
 1129 cropaleontology*, 70(1-2), 1–7.
- 1130 Lowenstein, T. K., Timofeeff, M. N., Brennan, S. T., Hardie, L. A., & Demicco,
 1131 R. V. (2001). Oscillations in Phanerozoic seawater chemistry: Evidence from
 1132 fluid inclusions. *Science*, 294(5544), 1086–1088.
- 1133 Malevich, S., Vetter, L., & Tierney, J. (2019). Global core top calibration of $\delta^{18}\text{O}$
 1134 in planktic foraminifera to sea-surface temperature. *Paleoceanography*. doi: 10
 1135 .1029/2019PA003576
- 1136 Marchitto, T. M., Muscheler, R., Ortiz, J. D., Carriquiry, J. D., & van Geen, A.
 1137 (2010). Dynamical response of the tropical Pacific Ocean to solar forcing
 1138 during the early Holocene. *Science*, 330(6009), 1378–1381.
- 1139 Mashiotta, T. A., Lea, D. W., & Spero, H. J. (1999). Glacial–interglacial changes in
 1140 Subantarctic sea surface temperature and $\delta^{18}\text{O}$ -water using foraminiferal Mg.
 1141 *Earth and Planetary Science Letters*, 170(4), 417–432.
- 1142 Mathien-Blard, E., & Bassinot, F. (2009). Salinity bias on the foraminifera Mg/Ca
 1143 thermometry: Correction procedure and implications for past ocean hydro-
 1144 graphic reconstructions. *Geochemistry, Geophysics, Geosystems*, 10(12).
- 1145 McConnell, M. C., & Thunell, R. C. (2005). Calibration of the planktonic
 1146 foraminiferal Mg/Ca paleothermometer: Sediment trap results from the Guay-
 1147 mas Basin, Gulf of California. *Paleoceanography and Paleoclimatology*, 20(2).
- 1148 Meland, M. Y., Jansen, E., Elderfield, H., Dokken, T. M., Olsen, A., & Bellerby,
 1149 R. G. (2006). Mg/Ca ratios in the planktonic foraminifer *Neogloboquadrina*
 1150 *pachyderma* (sinistral) in the northern North Atlantic/Nordic Seas. *Geochem-
 1151 istry, Geophysics, Geosystems*, 7(6).
- 1152 Mewes, A., Langer, G., de Nooijer, L. J., Bijma, J., & Reichert, G.-J. (2014). Ef-
 1153 fect of different seawater Mg^{2+} concentrations on calcification in two benthic
 1154 foraminifers. *Marine Micropaleontology*, 113, 56–64.
- 1155 Moffa-Sánchez, P., Hall, I. R., Barker, S., Thornalley, D. J., & Yashayaev, I. (2014).
 1156 Surface changes in the eastern Labrador Sea around the onset of the Little Ice
 1157 Age. *Paleoceanography*, 29(3), 160–175.
- 1158 Mohtadi, M., Oppo, D. W., Lückge, A., DePol-Holz, R., Steinke, S., Groeneveld, J.,
 1159 ... Hebbeln, D. (2011). Reconstructing the thermal structure of the upper
 1160 ocean: Insights from planktic foraminifera shell chemistry and alkenones in
 1161 modern sediments of the tropical eastern Indian Ocean. *Paleoceanography and
 1162 Paleoclimatology*, 26(3).
- 1163 Mohtadi, M., Steinke, S., Groeneveld, J., Fink, H. G., Rixen, T., Hebbeln, D., ...
 1164 Herunadi, B. (2009). Low-latitude control on seasonal and interannual changes
 1165 in planktonic foraminiferal flux and shell geochemistry off south Java: A sedi-
 1166 ment trap study. *Paleoceanography*, 24(1).
- 1167 Mohtadi, M., Steinke, S., Lückge, A., Groeneveld, J., & Hathorne, E. C. (2010).
 1168 Glacial to Holocene surface hydrography of the tropical eastern Indian Ocean.
 1169 *Earth and Planetary Science Letters*, 292(1), 89–97.
- 1170 Morley, A., Babila, T. L., Wright, J., Ninnemann, U., Kleiven, K., Irvali, N., &

- 1171 Rosenthal, Y. (2017). Environmental Controls on Mg/Ca in *Neogloboquadrina*
 1172 *incompta*: A Core-Top Study From the Subpolar North Atlantic. *Geochem-*
 1173 *istry, Geophysics, Geosystems*, 18(12), 4276–4298.
- 1174 Mortyn, P. G., & Charles, C. D. (2003). Planktonic foraminiferal depth habitat
 1175 and $\delta^{18}\text{O}$ calibrations: Plankton tow results from the Atlantic sector of the
 1176 Southern Ocean. *Paleoceanography*, 18(2).
- 1177 Mucci, A., & Morse, J. W. (1983). The incorporation of Mg^{2+} and Sr^{2+} into calcite
 1178 overgrowths: influences of growth rate and solution composition. *Geochimica et*
 1179 *Cosmochimica Acta*, 47(2), 217–233.
- 1180 Nürnberg, D., Bijma, J., & Hemleben, C. (1996). Assessing the reliability of magne-
 1181 sium in foraminiferal calcite as a proxy for water mass temperatures. *Geochim-*
 1182 *ica et Cosmochimica Acta*, 60(5), 803–814.
- 1183 Nürnberg, D., Ziegler, M., Karas, C., Tiedemann, R., & Schmidt, M. W. (2008).
 1184 Interacting Loop Current variability and Mississippi River discharge over the
 1185 past 400 kyr. *Earth and Planetary Science Letters*, 272(1-2), 278–289.
- 1186 O'Brien, C. L., Foster, G. L., Martínez-Botí, M. A., Abell, R., Rae, J. W., & Pan-
 1187 cost, R. D. (2014). High sea surface temperatures in tropical warm pools
 1188 during the Pliocene. *Nature Geoscience*, 7(8), 606–611.
- 1189 Oomori, T., Kaneshima, H., Maezato, Y., & Kitano, Y. (1987). Distribution coeffi-
 1190 cient of Mg^{2+} ions between calcite and solution at 10–50C. *Marine Chemistry*,
 1191 20(4), 327–336.
- 1192 Oppo, D. W., Rosenthal, Y., & Linsley, B. K. (2009). 2,000-year-long tempera-
 1193 ture and hydrology reconstructions from the Indo-Pacific warm pool. *Nature*,
 1194 460(7259), 1113–1116.
- 1195 Oppo, D. W., & Sun, Y. (2005). Amplitude and timing of sea-surface tempera-
 1196 ture change in the northern South China Sea: Dynamic link to the East Asian
 1197 monsoon. *Geology*, 33(10), 785–788.
- 1198 Pahnke, K., Zahn, R., Elderfield, H., & Schulz, M. (2003). 340,000-year centennial-
 1199 scale marine record of Southern Hemisphere climatic oscillation. *Science*,
 1200 301(5635), 948–952.
- 1201 Palmer, M., & Pearson, P. N. (2003). A 23,000-year record of surface water pH and
 1202 pCO₂ in the western equatorial Pacific Ocean. *Science*, 300(5618), 480–482.
- 1203 Parker, A. O., Schmidt, M. W., Jobe, Z. R., & Slowey, N. C. (2016). A new per-
 1204 spective on West African hydroclimate during the last deglaciation. *Earth and*
 1205 *Planetary Science Letters*, 449, 79–88.
- 1206 Pearson, P. N., van Dongen, B. E., Nicholas, C. J., Pancost, R. D., Schouten, S.,
 1207 Singano, J. M., & Wade, B. S. (2007). Stable warm tropical climate through
 1208 the Eocene Epoch. *Geology*, 35(3), 211–214.
- 1209 Raitzsch, M., Dueñas-Bohórquez, A., Reichart, G.-J., de Nooijer, L. J., & Bickert, T.
 1210 (2010). Incorporation of Mg and Sr in calcite of cultured benthic foraminifera:
 1211 impact of calcium concentration and associated calcite saturation state. *Bio-*
 1212 *geosciences*, 7(3), 869–881.
- 1213 Ravelo, A., & Fairbanks, R. (1992). Oxygen isotopic composition of multiple species
 1214 of planktonic foraminifera: Recorders of the modern photic zone temperature
 1215 gradient. *Paleoceanography and Paleoclimatology*, 7(6), 815–831.
- 1216 Regenberg, M., Nürnberg, D., Steph, S., Groeneveld, J., Garbe-Schönberg, D.,
 1217 Tiedemann, R., & Dullo, W.-C. (2006). Assessing the effect of dissolution
 1218 on planktonic foraminiferal Mg/Ca ratios: Evidence from Caribbean core tops.
 1219 *Geochemistry, Geophysics, Geosystems*, 7(7).
- 1220 Regenberg, M., Regenberg, A., Garbe-Schönberg, D., & Lea, D. W. (2014). Global
 1221 dissolution effects on planktonic foraminiferal Mg/Ca ratios controlled by the
 1222 calcite-saturation state of bottom waters. *Paleoceanography*, 29(3), 127–142.
- 1223 Regenberg, M., Steph, S., Nürnberg, D., Tiedemann, R., & Garbe-Schönberg, D.
 1224 (2009). Calibrating Mg/Ca ratios of multiple planktonic foraminiferal species
 1225 with $\delta^{18}\text{O}$ -calcification temperatures: Paleothermometry for the upper water

- 1226 column. *Earth and Planetary Science Letters*, 278(3-4), 324–336.
- 1227 Reynolds, L. A., & Thunell, R. C. (1986). Seasonal production and morphologic
1228 variation of *Neogloboquadrina pachyderma* (Ehrenberg) in the northeast Pa-
1229 cific. *Micropaleontology*, 32, 1–18.
- 1230 Richey, J. N., Poore, R. Z., Flower, B. P., & Hollander, D. J. (2012). Ecological
1231 controls on the shell geochemistry of pink and white globigerinoides ruber in
1232 the northern gulf of mexico: Implications for paleoceanographic reconstruction.
1233 *Marine Micropaleontology*, 82-83(C), 28–37.
- 1234 Richey, J. N., Poore, R. Z., Flower, B. P., & Quinn, T. M. (2007). 1400 yr multi-
1235 proxy record of climate variability from the northern Gulf of Mexico. *Geology*,
1236 35(5), 423–426.
- 1237 Richey, J. N., Poore, R. Z., Flower, B. P., Quinn, T. M., & Hollander, D. J. (2009).
1238 Regionally coherent little ice age cooling in the Atlantic warm pool. *Geophys-
1239 ical Research Letters*, 36(21).
- 1240 Richey, J. N., Thirumalai, K., Khider, D., Reynolds, C. E., Partin, J. W., & Quinn,
1241 T. M. (2019). Considerations for Globigerinoides ruber (White and Pink)
1242 Paleocyanography: Comprehensive Insights From a Long-Running Sediment
1243 Trap. *Paleoceanography and Paleoclimatology*, 34, 353–373.
- 1244 Riethdorf, J.-R., Max, L., Nürnberg, D., Lembke-Jene, L., & Tiedemann, R. (2013).
1245 Deglacial development of (sub) sea surface temperature and salinity in the
1246 subarctic northwest Pacific: Implications for upper-ocean stratification. *Paleo-
1247 ceanography*, 28(1), 91–104.
- 1248 Romahn, S., Mackensen, A., Groeneveld, J., & Pätzold, J. (2014). Deglacial inter-
1249 mediate water reorganization: new evidence from the Indian Ocean. *Climate of
1250 the Past*, 10(1), 293–303.
- 1251 Rosenthal, Y., & Boyle, E. A. (1993). Factors controlling the fluoride content of
1252 planktonic foraminifera: An evaluation of its paleoceanographic applicability.
1253 *Geochimica et Cosmochimica Acta*, 57(2), 335–346.
- 1254 Rosenthal, Y., Lohmann, G., Lohmann, K., & Sherrell, R. (2000). Incorporation
1255 and preservation of Mg in Globigerinoides sacculifer: Implications for recon-
1256 structing the temperature and $^{18}\text{O}/^{16}\text{O}$ of seawater. *Paleoceanography*, 15(1),
1257 135–145.
- 1258 Rosenthal, Y., & Lohmann, G. P. (2002). Accurate estimation of sea surface temper-
1259 atures using dissolution-corrected calibrations for Mg/Ca paleothermometry.
1260 *Paleoceanography*, 17(3).
- 1261 Rosenthal, Y., Oppo, D. W., & Linsley, B. K. (2003). The amplitude and phasing of
1262 climate change during the last deglaciation in the sulu sea, western equatorial
1263 pacific. *Geophysical Research Letters*, 30(8).
- 1264 Rosenthal, Y., Perron-Cashman, S., Lear, C. H., Bard, E., Barker, S., Billups, K.,
1265 ... Wilson, P. A. (2004). Interlaboratory comparison study of Mg/Ca and
1266 Sr/Ca measurements in planktonic foraminifera for paleoceanographic research.
1267 *Geochemistry, Geophysics, Geosystems*, 5(4).
- 1268 Russell, A. D., Emerson, S., Nelson, B. K., Erez, J., & Lea, D. W. (1994). Ura-
1269 nium in foraminiferal calcite as a recorder of seawater uranium concentrations.
1270 *Geochimica et Cosmochimica Acta*, 58(2), 671–681.
- 1271 Russell, A. D., Hönisch, B., Spero, H. J., & Lea, D. W. (2004). Effects of seawater
1272 carbonate ion concentration and temperature on shell U, Mg, and Sr in
1273 cultured planktonic foraminifera. *Geochimica et Cosmochimica Acta*, 68(21),
1274 4347–4361.
- 1275 Rustic, G. T., Koutavas, A., Marchitto, T. M., & Linsley, B. K. (2015). Dynamical
1276 excitation of the tropical Pacific Ocean and ENSO variability by Little Ice Age
1277 cooling. *Science*, 350, 1537–1541.
- 1278 Sabbatini, A., Bassinot, F., Boussetta, S., Negri, A., Rebaubier, H., Dewilde, F., ...
1279 Morigi, C. (2011). Further constraints on the diagenetic influences and salinity
1280 effect on Globigerinoides ruber (white) Mg/Ca thermometry: Implications in

- 1281 the Mediterranean Sea. *Geochemistry, Geophysics, Geosystems*, 12(10).
- 1282 Sadekov, A. Y., Darling, K. F., Ishimura, T., Wade, C. M., Kimoto, K., Singh,
1283 A. D., ... others (2016). Geochemical imprints of genotypic variants of *Glo-*
1284 *bigerina bulloides* in the Arabian Sea. *Paleoceanography*, 31(10), 1440–1452.
- 1285 Saenger, C. P., & Evans, M. N. (2019). Calibration and validation of environmen-
1286 tal controls on planktic foraminifera Mg/Ca using global core-top data. *Paleo-*
1287 *ceanography and Paleoclimatology*. doi: 10.1029/2018PA003507
- 1288 Saraswat, R., Lea, D. W., Nigam, R., Mackensen, A., & Naik, D. K. (2013).
1289 Deglaciation in the tropical Indian Ocean driven by interplay between the
1290 regional monsoon and global teleconnections. *Earth and Planetary Science*
1291 *Letters*, 375, 166–175.
- 1292 Schmidt, M. W., Chang, P., Hertzberg, J. E., Them, T. R., Ji, L., & Otto-Bliesner,
1293 B. L. (2012). Impact of abrupt deglacial climate change on tropical Atlantic
1294 subsurface temperatures. *Proceedings of the National Academy of Science*,
1295 109, 14348–14352.
- 1296 Schmidt, M. W., Spero, H. J., & Lea, D. W. (2004). Links between salinity vari-
1297 ation in the Caribbean and North Atlantic thermohaline circulation. *Nature*,
1298 428(6979), 160–163.
- 1299 Schmidt, M. W., Weinlein, W. A., Marcantonio, F., & Lynch-Stieglitz, J. (2012). So-
1300 lar forcing of Florida Straits surface salinity during the early Holocene. *Paleo-*
1301 *ceanography*, 27(3).
- 1302 Segev, E., & Erez, J. (2006). Effect of Mg/Ca ratio in seawater on shell composition
1303 in shallow benthic foraminifera. *Geochemistry, Geophysics, Geosystems*, 7(2).
- 1304 Sjöberg, E. (1976). A fundamental equation for calcite dissolution kinetics. *Geochim-*
1305 *ica et Cosmochimica Acta*, 40(4), 441–447.
- 1306 Steinke, S., Chiu, H.-Y., Yu, P.-S., Shen, C.-C., Löwemark, L., Mii, H.-S., & Chen,
1307 M.-T. (2005). Mg/Ca ratios of two *Globigerinoides ruber* (white) morpho-
1308 types: Implications for reconstructing past tropical/subtropical surface water
1309 conditions. *Geochemistry, Geophysics, Geosystems*, 6(11).
- 1310 Steinke, S., Kienast, M., Groeneveld, J., Lin, L.-C., Chen, M.-T., & Rendle-Bühring,
1311 R. (2008). Proxy dependence of the temporal pattern of deglacial warming
1312 in the tropical South China Sea: toward resolving seasonality. *Quaternary*
1313 *Science Reviews*, 27(7), 688–700.
- 1314 Stott, L., Timmermann, A., & Thunell, R. (2007). Southern hemisphere and deep-
1315 sea warming led deglacial atmospheric CO₂ rise and tropical warming. *science*,
1316 318(5849), 435–438.
- 1317 Sun, Y., Oppo, D. W., Xiang, R., Liu, W., & Gao, S. (2005). Last deglaciation in
1318 the Okinawa Trough: Subtropical northwest Pacific link to Northern Hemi-
1319 sphere and tropical climate. *Paleoceanography*, 20(4).
- 1320 Taylor, B. J., Rae, J. W., Gray, W. R., Darling, K. F., Burke, A., Gersonde, R.,
1321 ... Ziveri, P. (2018). Distribution and ecology of planktic foraminifera in
1322 the North Pacific: Implications for paleo-reconstructions. *Quaternary Science*
1323 *Reviews*, 191, 256–274.
- 1324 Thirumalai, K., Quinn, T. M., & Marino, G. (2016). Constraining past seawater
1325 $\delta^{18}\text{O}$ and temperature records developed from foraminiferal geochemistry. *Pa-*
1326 *leoceanography*, 31(10), 1409–1422.
- 1327 Thornalley, D. J., Elderfield, H., & McCave, I. N. (2011). Reconstructing North
1328 Atlantic deglacial surface hydrography and its link to the Atlantic overturning
1329 circulation. *Global and Planetary Change*, 79(3-4), 163–175.
- 1330 Tierney, J. E., Pausata, F. S., & deMenocal, P. (2016). Deglacial Indian monsoon
1331 failure and North Atlantic stadials linked by Indian Ocean surface cooling. *Nature*
1332 *Geoscience*, 9(1), 46–50.
- 1333 Tierney, J. E., & Tingley, M. P. (2014). A Bayesian, spatially-varying calibration
1334 model for the TEX₈₆ proxy. *Geochimica et Cosmochimica Acta*, 127, 83–106.
- 1335 Tierney, J. E., & Tingley, M. P. (2018). BAYSPLINE: A new calibration for the

- 1336 alkenone paleothermometer. *Paleoceanography and Paleoclimatology*, *33*(3),
 1337 281–301.
- 1338 Tripathi, A. K., Delaney, M. L., Zachos, J. C., Anderson, L. D., Kelly, D. C., & Elder-
 1339 field, H. (2003). Tropical sea-surface temperature reconstruction for the early
 1340 Paleogene using Mg/Ca ratios of planktonic foraminifera. *Paleoceanography*,
 1341 *18*(4).
- 1342 Tyrrell, T., & Zeebe, R. E. (2004). History of carbonate ion concentration over the
 1343 last 100 million years. *Geochimica et Cosmochimica Acta*, *68*(17), 3521–3530.
- 1344 Žarić, S., Donner, B., Fischer, G., Mulitza, S., & Wefer, G. (2005, April). Sensitiv-
 1345 ity of planktic foraminifera to sea surface temperature and export production
 1346 as derived from sediment trap data. *Marine Micropaleontology*, *55*(1), 75–
 1347 105. Retrieved 2018-03-28, from [http://www.sciencedirect.com/science/
 1348 article/pii/S0377839805000186](http://www.sciencedirect.com/science/article/pii/S0377839805000186) doi: 10.1016/j.marmicro.2005.01.002
- 1349 Van Heuven, S., Pierrot, D., Rae, J., Lewis, E., & Wallace, D. (2011). Matlab
 1350 program developed for co₂ system calculations. *ORNL/CDIAC-105b. Carbon
 1351 Dioxide Information Analysis Center, Oak Ridge National Laboratory, US
 1352 Department of Energy, Oak Ridge, Tennessee*, 530.
- 1353 van Raden, U. J., Groeneveld, J., Raitzsch, M., & Kucera, M. (2011). Mg/Ca in
 1354 the planktonic foraminifera *Globorotalia inflata* and *Globigerinoides bulloides*
 1355 from Western Mediterranean plankton tow and core top samples. *Marine
 1356 Micropaleontology*, *78*(3-4), 101–112.
- 1357 Vázquez Riveiros, N., Govin, A., Waelbroeck, C., Mackensen, A., Michel, E., Mor-
 1358 eira, S., ... Brandon, M. (2016). Mg/Ca thermometry in planktic foraminifera:
 1359 Improving paleotemperature estimations for *G. bulloides* and *N. pachyderma*
 1360 left. *Geochemistry, Geophysics, Geosystems*, *17*(4), 1249–1264.
- 1361 Vehtari, A., Gelman, A., & Gabry, J. (2017). Practical Bayesian model evalua-
 1362 tion using leave-one-out cross-validation and WAIC. *Statistics and Computing*,
 1363 *27*(5), 1413–1432.
- 1364 Visser, K., Thunell, R., & Stott, L. (2003). Magnitude and timing of temperature
 1365 change in the indo-pacific warm pool during deglaciation. *Nature*, *421*(6919),
 1366 152–155.
- 1367 Von Langen, P. J., Pak, D. K., Spero, H. J., & Lea, D. W. (2005). Effects of temper-
 1368 ature on Mg/Ca in neogloboquadrinid shells determined by live culturing. *Geo-
 1369 chemistry, Geophysics, Geosystems*, *6*(10).
- 1370 Wara, M. W., Ravelo, A. C., & Delaney, M. L. (2005). Permanent El Niño-like con-
 1371 ditions during the Pliocene warm period. *Science*, *309*(5735), 758–761.
- 1372 Wei, G., Deng, W., Liu, Y., & Li, X. (2007). High-resolution sea surface tempera-
 1373 ture records derived from foraminiferal Mg/Ca ratios during the last 260 ka in
 1374 the northern South China Sea. *Palaeogeography, Palaeoclimatology, Palaeoecol-
 1375 ogy*, *250*(1), 126–138.
- 1376 Weldeab, S., Lea, D. W., Oberhänsli, H., & Schneider, R. R. (2014). Links between
 1377 southwestern tropical Indian Ocean SST and precipitation over southeastern
 1378 Africa over the last 17 kyr. *Palaeogeography, palaeoclimatology, palaeoecology*,
 1379 *410*, 200–212.
- 1380 Weldeab, S., Lea, D. W., Schneider, R. R., & Andersen, N. (2007). 155,000 years of
 1381 West African monsoon and ocean thermal evolution. *science*, *316*(5829), 1303–
 1382 1307.
- 1383 Weldeab, S., Schneider, R., & Kölling, M. (2006). Deglacial sea surface temperature
 1384 and salinity increase in the western tropical Atlantic in synchrony with high
 1385 latitude climate instabilities. *Earth and Planetary Science Letters*, *241*(3),
 1386 699–706.
- 1387 Weldeab, S., Schneider, R. R., Kölling, M., & Wefer, G. (2005). Holocene African
 1388 droughts relate to eastern equatorial Atlantic cooling. *Geology*, *33*(12), 981–
 1389 984.
- 1390 Xu, J., Kuhnt, W., Holbourn, A., Regenberg, M., & Andersen, N. (2010). Indo-

- 1391 Pacific warm pool variability during the Holocene and Last Glacial Maximum.
1392 *Paleoceanography*, 25(4).
- 1393 Yu, J., Elderfield, H., Jin, Z., & Booth, L. (2008). A strong temperature effect
1394 on U/Ca in planktonic foraminiferal carbonates. *Geochimica et Cosmochimica*
1395 *Acta*, 72(20), 4988–5000.
- 1396 Zhang, Y. G., Pagani, M., & Liu, Z. (2014). A 12-million-year temperature history
1397 of the tropical Pacific Ocean. *Science*, 344(6179), 84–87.
- 1398 Zhu, J., Poulsen, C. J., & Tierney, J. E. (2019). Simulation of Eocene extreme
1399 warmth and high climate sensitivity through cloud feedbacks. *Science Ad-*
1400 *vances*, accepted. doi: 10.1126/sciadv.aax1874